Computational Assessments on Bubble Dynamics Applied to Flotation Cells

by

Asif Mammadov

A thesis submitted in partial fulfillment of the requirements for the degree of

Master of Science

in
chemical engineering

Department of Chemical and Materials Engineering
University of Alberta

Unsteady mind is like mercury, liquid metal moving all the time, if one can stop and focus, it turns to silver and when one finds love, at this moment it turns to gold.

Golden key of Alchemy

Abstract

Au, Ag, Hg, many other metals, diamond, coal, oil and tar sands are extracted by flotation process. We can define flotation as a single, most significant unit operation in mineral processing, used in extraction of all kinds of minerals. A study of air bubble dynamics and gas-liquid multiphase flow is important for the design, development and understanding of industrial processes such as bubble column reactors, flotation cells and boilers. Hence bubble generation and attachment is an important part of flotation process. In order to understand bubble dynamics, we built models of single bubble systems. The growth and detachment of air bubble from single orifice in water tank was studied. An axisymmetric model based on the Volume of Fluid method, available in ANSYS-Fluent software was used for simulation of air bubble rising in water. Numerous numerical simulations were carried out using an axisymmetric domain with different orifice diameters (0.8, 0.4 mm), air inlet velocities (50, 150 mlph) and phase surface tensions (50, 72 mN/m). Bubble growth and rise velocity were studied and validated against experimental data published in literature. Relative good agreement was achieved. Velocity profiles of the rising bubbles as well as Reynolds, Weber and Capillary numbers were calculated. Effect of surface tension and nozzle diameter to bubble size and dynamics were discussed. It was shown that smaller surface tension of the system yields to smaller bubble size which is more favorable for flotation process.

Aknowledgements

First of all I would like to thank my parents for their unconditional love and support. Important as parental support, guidance of masters and teachers is what makes possible travel through the enlightening path called science. I would like to express my sincere gratitude to my supervisors Dr. Petr Nikrityuk and Dr. Zhenghe Xu for their invaluable guidance, help and for their support at University of Alberta. Thanks to Dr. Rogerio Manica for his friendly advices. Thanks to secretaries Ms. Lily Laser and Ms. Lisa Carreiro, for their professional approach. Also I would like to thank Mr. Jim Skwarok for being helpful in every situation

Table of contents

List of |tables

List of figures

Nomenclature

$\vec{v}$: fluid velocity (m/s)

p: pressure (Pa),

μ: viscosity (Pa·s),

ρ: density (kg/m^3)

ρ_g: gas density (kg/m^3)

ρ_l :liquid density (kg/m^3)

ε: volume fraction

γ: surface tension (N/m)

g: gravitational acceleration (m/s^2),

t$_i$: induction time

k: curvature

u_t : bubble rising velocity

F: volumetric surface tension force

We: Weber number

Ca; Capillary number

Re: Reynolds number

CV: Control volumes

D: diameter of bubble (m),

Z: height of tank (m),

r: radius of tank (m)

L: width of tank

Chapter 1 Analysis of flotation modeling

Section 1.1 Froth flotation

Flotation is a separation process used in mineral extraction and works by concentration of one kind of particles from another by their selective attachment onto the fluid interfaces [1]. In ore processing froth flotation is believed to be the most extensively used application. In this process essential minerals are separated from soil by gathering them on the surface layer of froth. Froth flotation is a complex physicochemical process used in mineral extraction to separate valuable minerals from gangue in low-grade ores. Most kind of metals, sulfide minerals are regained by using froth flotation process. Firstly flotation cells were used for separation of sulfide minerals from gangue, later many other minerals are also extracted by this process. Nowadays beside mineral extraction flotation cells are used in different fields such as wastewater treatment, protein separation, odor removal, deinking of used paper, separation and harvesting of microorganisms, clarification of fruit juices and so on [2]. The ability of certain chemicals to modify surface properties of other substances is widely used in flotation process. The flotation process depends in control of the pulp chemistry to increase the hydrophobicity of the valuable minerals. Adjustment of pH value of the system is also very important and buffer type solutions were generated to keep acidity level in control. Also some other chemicals are used to generate stable froth. Hence bubble behavior plays important role, the efficiency is also highly affected by the hydrodynamics and gas dispersion in the flotation cell [3]. In froth flotation, hydrophobic particles are separated by attaching themselves to rising air bubbles to form a particle-rich froth on the suspension surface as shown in Figure1.1. Particles can be hydrophobic in nature, in this case air bubbles are attached to them easily. In the mixture of hydrophobic and hydrophilic particles, air bubbles tend to attach to hydrophobic ones. By addition of chemicals the hydrophobicity of the particles can be increased.

The characteristics of some chemicals to change surface properties of the system is used in froth flotation.
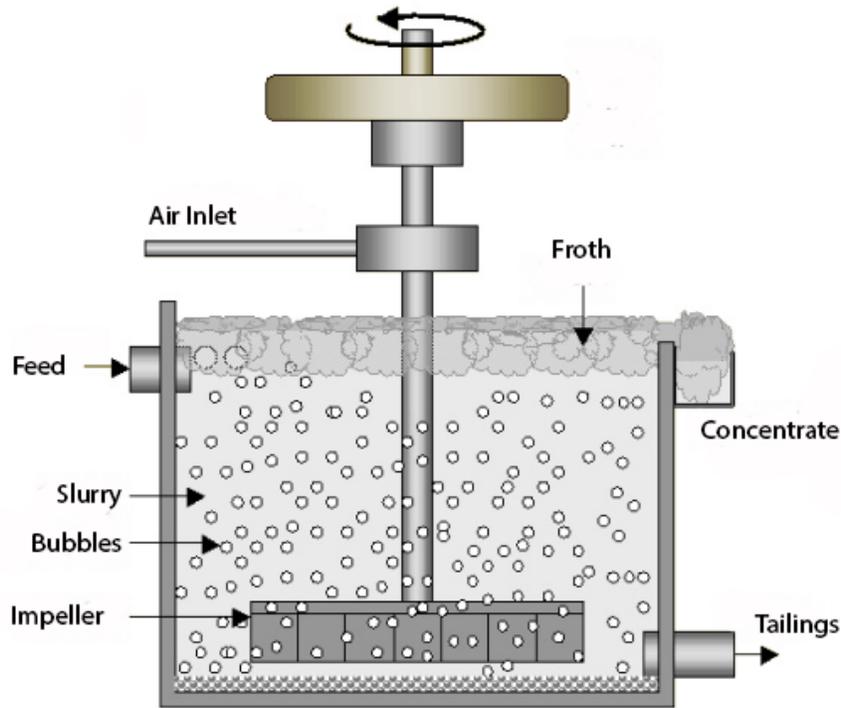
Figure 1.1 General scheme of flotation process, feed given from left is mixed by impeller and generated air bubbles are connected to the hydrophobic particles to form particle rich froth, reproduced from [4]

The surface properties of the minerals play an important role on its floating ability. As air attachment is important part of the flotation process and depends on minerals surface properties, some chemical modifications for better attachment purposes are conducted. After the contact with mineral surfaces air bubbles rise to generate particle rich froth. Once reached the surface, air bubbles collide but the mineral stays on the froth surface. Next the froth minerals are concentrated and separated from the remaining part and send to further cleaning.

Flotation is used by chemical and mineral engineers for the concentration and separation of aqueous suspensions or solutions of a variety of minerals, coal, precipitates, inorganic waste

constituents, effluents, and also proteins and microorganisms. It is supposed that worldwide more than two billion tons of various minerals and are coal annually treated by flotation process. This number, represents approximately 85% of minerals mined annually [5], will be increased in the future with the utilization of high-grade ore deposits. Flotation of coal also significantly increments due to the increased mechanization of beneficiation methods that manufactures significant amounts of fine coal particles.

The framework of flotation technology has been extended into many other areas of engineering, such as wastepaper deinking for recycling, separation of plastics and water treatment. At the present time in worldwide paper production flotation deinking annually endows about 130 million tons of recovered paper. This number correlates to about half of the annual papermaking quantity [5].

Mineral processing, wastepaper deinking, water treatment, plastic treatment technologies are considered as the main industries where flotation process is used.

Section 1.2 Flotation Mechanics and Reagents

Induced air flotation is the process where air bubbles used as carriers, attached to the target components in a complex multiphase system. In induced mechanical flotation cells bubble-bitumen attachment in slurry occurs. In dissolved air flotation bubble nucleation of bitumen takes place. A mechanical flotation machine consists of the following attributes [6]:

1) Mechanical agitator hosted in a standpipe and used to homogenize the slurry and suspend the solids

2) Feed mechanism to introduce the feed slurry into the apparatus

3) Air/gas supplier of for the generation of bubbles;

4) Quiescent region for aerated bitumen to float;

5) A mechanism to remove the aerated bitumen froth;

6) A tailings discharge mechanism to discharge tailings without short-circuiting the feed slurries.

Bubbles are an essential fundamental of froth flotation process. Bubble propagation in flotation machines forms the second base of a mineral flotation system. It is important to note that the advancement of flotation cells follows the transformation of bubble generation methods, although a flotation machine has to fulfill three main principles [7]:

a) Origination of plentiful amount of bubbles with relevant sizes (0.5–2 mm);

b) Dispersion of solid materials;

c) Efficient collision between particles and bubbles, in addition to providing a quiescent zone for froth formation.

The bubble size generated during flotation process has a great effect on productivity of flotation and separation process in general [8]. Fine mineral particles can only be separated by the relevant size of air bubbles.

Based on their role, flotation reagents are classified as collectors, frothers and modifiers. All three types of reagents have critical roles and importance, and are involved in complex interactions. Flotation reagents have two important structural features: a functional group consisting of donor atoms or ligands, and a substituent group. The functional group is hydrophobic consisting of alkyl aryl hydrocarbon chains in the case of collectors and frothers, or hydrophilic in the case of modifiers [9]. Xanthate and dithiophosphate are more generic collectors and used in large tonnages. Two important families of alcohols are used as frother, the short-chain aliphatic alcohols and polyglycols (unsubstituted or alkyl monoethers).

Section 1.3 Flotation of oil sands ore

Water-based flotation process has long been used for the separation of bitumen from surface mined oil sands. Bituminous froths, which represent a special class of non-aqueous foams and are multi-phase, and composed of oil, solids, water and gas is produced during flotation [10]. Both the nature of the original oil or tar sands and the manner in which the oil sand conditioning and separation processes are conducted effect the properties of the froths. Bitumen obtained from the froths is converted into fuels and other products. The properties of these froths also influence the subsequent downstream processing steps.

One of the main issues for separation in oil sands and generally in flotation is attachment probability of air bubbles to bitumen.

For attachment probability analysis equation derived by Yoon and Luterall is adopted [11]. Some assumptions were made, like interaction of bitumen particles between each other and hydrodynamic forces are neglected. To calculate attachment probability of the bubbles to bitumen surface next equation is used:

$$P_a = sin^2[2arctan \cdot \exp(\frac{(45+8Re^{0.72})V_b t_i}{15D_b(\frac{D_b}{D_p}+1)})] \qquad (1.1)$$
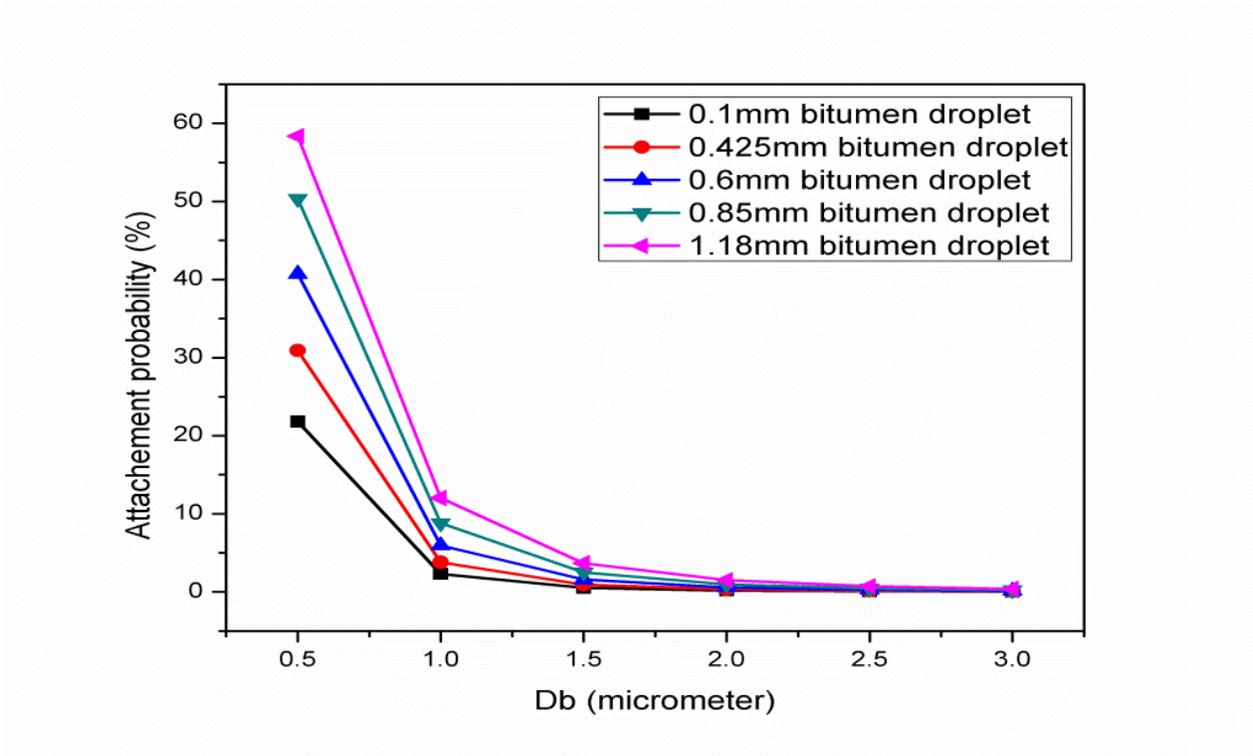
Figure 1.2 Attachment probability of air bubbles with different diameter to various sized bitumen

For building the model and calculations, we assume that induction time is 0.001s for all cases. As it is seen from figure 4 attachment probabilities of bubbles dramatically increases when the size of bubbles are smaller than 1 micron. Also it is seen that, smaller sized bubbles are more probably attached to big sized bitumen droplets.

After attaching bubbles to mineral surface it is also important that it doesn't detach after some point but rise to the froth for separation. It is important for froth quality. Detachment of the air bubbles from mineral surface may occur during turbulence flows. In this regard flotation column is more favorable for separation of coarse particles rather than mechanical flotation cell. For detachment probability calculations derived equation for bitumen particles are used [12]:

$$P_d = \frac{20461 D_p^2 D_b}{\left(20461 D_p^2 D_b\right) + 0.1437(D_b + D_p)} \qquad (1.2)$$
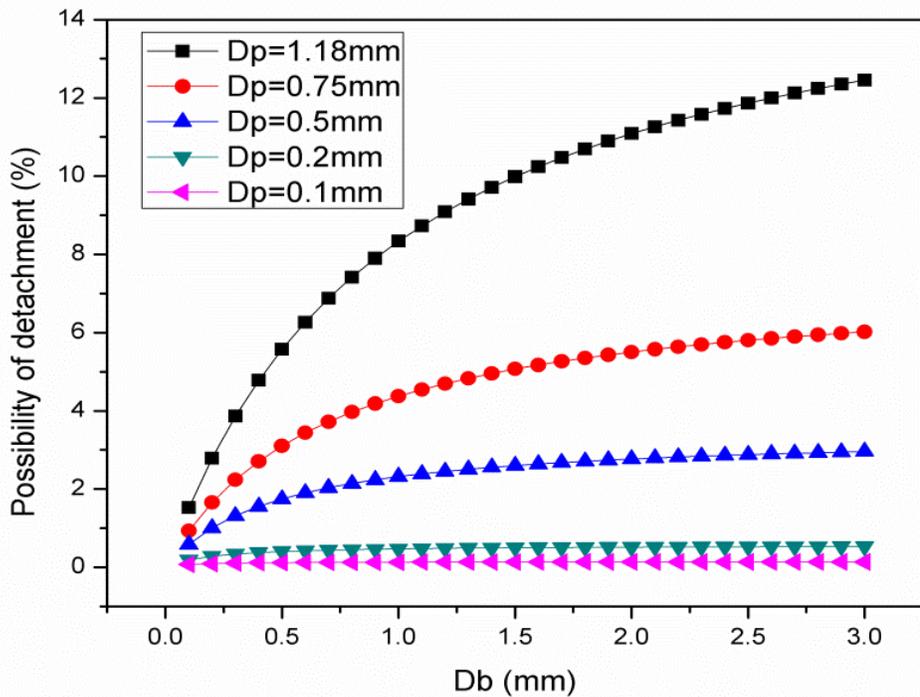
Figure 1.3 Detachment probability *vs* bubble diameter for different bitumen particle size

Results of calculations for detachment probability and bubble diameter relationship for different bitumen droplets are shown in figure 1.3. The same assumptions as in case of attachment probabilities calculations were made. In flotation process for stability of the froth detachment is not wanted. So as it is seen from the figures small sized bubbles are attached very well and detachment probabilities for them is lower compared to bigger sized bubbles.

Beside attachment and detachment probabilities, it has been shown that smaller bubbles need less time to attach to bitumen surface compared to bigger ones [13]. This time is called induction time and plays important role in effective bubble bitumen interaction. Bubbles generated in the flotation cell have limited time to attach to the hydrophobic surface. Experiments conducted by using hydrogen bubbles have shown that there is a critical diameter of bubbles after which no attachment to hydrophobic surface is manifested.
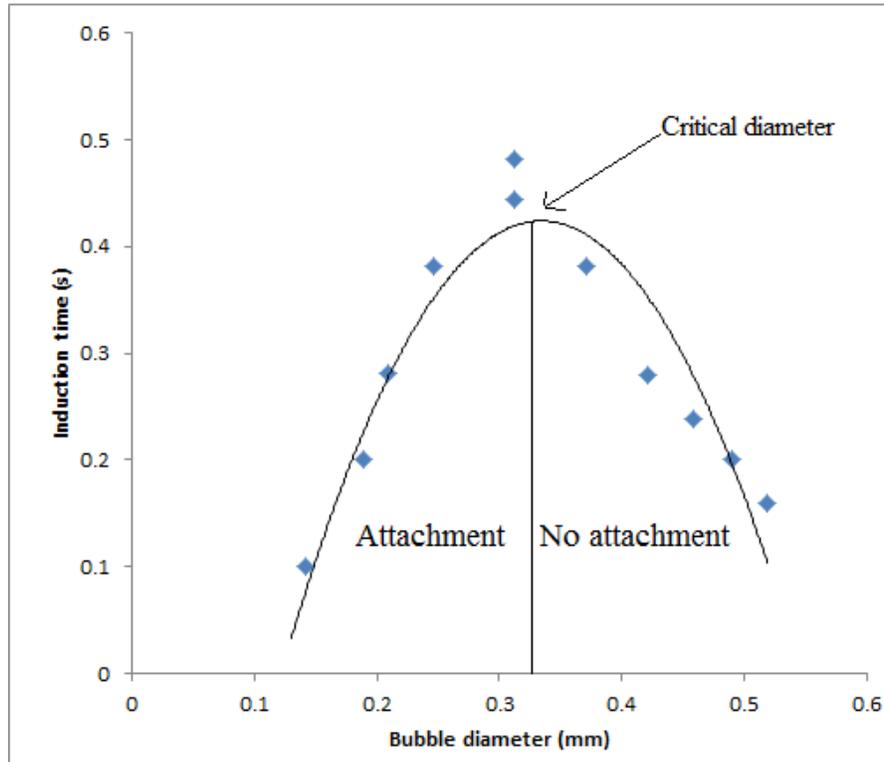
Figure 1.4 Experimental analysis of induction time of Hydrogen bubble against bitumen surface in deaerated municipal water at 50 °C, redrawn from source [13]

In case of Hydrogen it was established that bubbles smaller than 0.32 mm diameter attach to bitumen surface and smaller bubbles attach more rapidly. As it is seen from figure 1.4 induction times are less in case with smaller bubble size. Fast attachment of bubbles to bitumen surface is important because in flotation process the time for bubbles to connect to mineral surfaces is limited. Speed of bubbles travelling from bottom of the flotation machine to the top can be decreased by using chemical additives. Also small bubbles travel with less speed compared to big ones, which give more time for collision with mineral surfaces.

Section 1.4 Computational Fluid Dynamics in flotation

Considering that flotation is a complex multiphase process, computational fluid dynamics simulation of this matter is relatively challenging problem and in literature most of the works are

done in XXI century. As we described above, productivity of the flotation process is dependent on bubble mineral collisions and formation of stable froth. In this view, CFD simulation of bubble-particle collisions in mineral flotation cells was provided [14]. The efficiency of the floatation processes is highly dependent on the initial contact between bubbly and particle. By means of CFD simulation of floatation cells, the influence of design and operating conditions can be predicted in advance. In the simulation described above laboratory floatation cell designed by CSIRO Minerals and cylindrical tank filled with a Rushtone type turbine were modelled for comparison. Impeller and cell geometries were built by using the multi blocking and sliding mesh techniques. 3D profiles of the turbulence dissipation rate and volumetric fraction of the air are obtained in order to determine bubble-particle collisions per unit time and unit volume. These profiles are significantly important in terms of defining the location positions within floatation cells where the initial contacts between bubbles and particles are formed. Collision rate which define efficiency of the floatation process and in this view CSIRO floatation cell and stirred tank were compared to each other. Based on the results, it was revealed that CSIRO floatation cell is superior for floatation compared to stirred tank with Rushtone turbine. It can be added that, the collision rate distributions calculated by CFD were essential tool for locating position within floatation cells which helps to understand floatation process and advance design modifications. This will subsequently lead to increasing floatation performance in general.

In different work of the same authors, computational fluid dynamic (CFD) modelling of a Denver-type flotation cell was performed [15]. Bubble–particle collision rates in different positions of the cell were calculated based on the local turbulent velocities, and the size and numbers of bubbles and concentrations of particles were obtained from CFD modelling. The collision probability which is caused by streamline effect of fine particles moving around the bubble was also been

evaluated. Moreover, the local attachment rate based on the collision rate was found to change disproportionally with particle size. On the other hand normalized collision rate is rather insensitive to particle size. This finding is highly consistent with the decrease in flotation recovery of fine particles as observed in flotation practice in general. The magnitudes of the collection rate constants extracted from CFD modelling represents that transport rates of the bubble-particle aggregates to the froth layer may have a significant contribution to the overall flotation rate in plant-scale equipment.

In a different work computational fluid dynamics model was developed to understand effect of induction time and stirring speed on flotation cell. For this purpose a modified Denver flotation cell used in laboratory batch tests [16]. The model was proposed to incorporate fundamental aspects of bubble-particle interactions including bubble-particle collision, attachment and detachment. Results from the modeling were compared against laboratory experiments of flotation cell with narrowly-sized spherical ballotini. For both cases flotation results for different impeller speeds were obtained with a constant air flow into the cell. For a given particle size, the results obtained from the modeling and experimental work indicated that there was an optimum stirring speed that makes a balance between attachment and detachment rates in the cell for flotation. The hydrophobic particles were obtained by methylation of ballotini with trimethylchlorosilane. It was shown that in case of less hydrophobic particles, relatively lower stirring speed is more advantageous to have a longer contact time which was attributed to the longer induction time required for attachment [14].

The results of CFD simulations of the CSIRO batch flotation cell (a modified Denver cell) were verified against measurements from carefully planned batch flotation tests. The simulation results contain detailed information for the liquid velocity vectors, void fraction and turbulent energy

dissipation rates in the cell at three different impeller stirring speeds: 1050, 1200 and 1500 rpm. It was found that the average gas holdup in the cell is inclined to decrease with reducing stirring speed and the final values were in well agreement with observations with the increased height of the pulp surface occurs when air flow is pumped into the cell. Considering the local turbulent energy dissipation rate is one of major factors which controls both the attachment and detachment rates, contour distributions of the turbulent energy dissipation rate at three stirring speeds and the volume distribution of the turbulent energy dissipation rate in the cell were obtained for simulating flotation. Flotation kinetics was simulated for fully methylated ballotini. The net attachment rates appeared to be different across the flotation cell due to varying hydrodynamics in different parts of the cell. In regions of the cell where net attachment values are negative, the local detachment rate exceeded the local attachment rate. Overall, the predicted and measured recovery-time curves are in good agreement at the three stirring speeds which were studied. This is confirmed by both the flotation rate constant and the cumulative recovery values for fully methylated ballotini particles. For less hydrophobic particles, a lower stirring speed can provide a longer sliding time since it is required for efficient attachment [16].

Bubble–particle collision efficiency in a turbulent flow was studied from a perspective of multiscale modelling [17]. An integrated CFD-based scheme was developed in order to predict the efficiency of turbulent bubble–particle collision. Meanwhile, the effect of turbulence and the bubble wall effect on bubble–particle collision efficiency was systematically studied by using a 3D low turbulent Reynolds number shear-stress-transport turbulence model. Example simulations and comparisons were carried out to illustrate the methodology. This method can also be applied to non-Newtonian slurries.

A CFD model which constitutes flotation kinetic expressions was developed to simulate the performance of flotation tanks utilized in water and wastewater treatment plants [18]. Dissolved Air Flotation (DAF) tanks, where bubble buoyancy, particle settling and turbulence are mechanisms contributing comparably to local flotation rates were modelled. This study was mainly focused on tanks that are able to operate without any external means of flow mixing. These flotation mechanisms were carefully analyzed, and their relative contribution with respect to basic parameters of the flotation process was investigated. Some assumptions were made regarding the fluid dynamics and particle conservation issues of the developed model to increase the efficiency of computations, and CFD simulations were performed in a two-dimensional frame of reference. Finally simulation results revealed the existence of a complex interaction between tank hydrodynamics and local flotation rates which lead to particle removal efficiencies.

Certain mineral slurries especially with finer particle size and high solid concentration used in the minerals processing industry have been shown to exhibit non-Newtonian rheology [19]. Research has also shown that a cavern surrounded by stagnant fluid form around the impeller during the agitation of non-Newtonian fluids exhibiting yield stresses, and this is therefore hypothesized to take place inside mechanical flotation cells which may negatively affect fluid hydrodynamics. A single phase non-Newtonian fluids was modelled using CFD by using the Herschel-Bulkley non-Newtonian model with constants that derived from experimentally determined Bindura nickel ore slurry which known as rheological complex due to the presence of fibrous mineral types, such as serpentine. The modelling methodology was first confirmed with published experimental results in a stirred tank, and results were experimentally validated using piezoelectric pressure transducers to measure the magnitude of pressure changes arising from the fluid velocity in order to specify the cavern boundary. Both experimental and numerical findings show that a cavern forms around

the stator and its size closely depends on slurry yield stress. It was also found that the shear–stress transport (SST) k-ωk-ω turbulence model predicted the cavern boundary most accurately.

CFD simulations were conducted in order to investigate the effects of non-Newtonian mineral slurry rheology on the hydrodynamics inside a mechanical flotation cell. The modelling methodology used was first validated by modelling a pitch-blade turbine agitated tank and comparing results against published experimental cavern measurements.
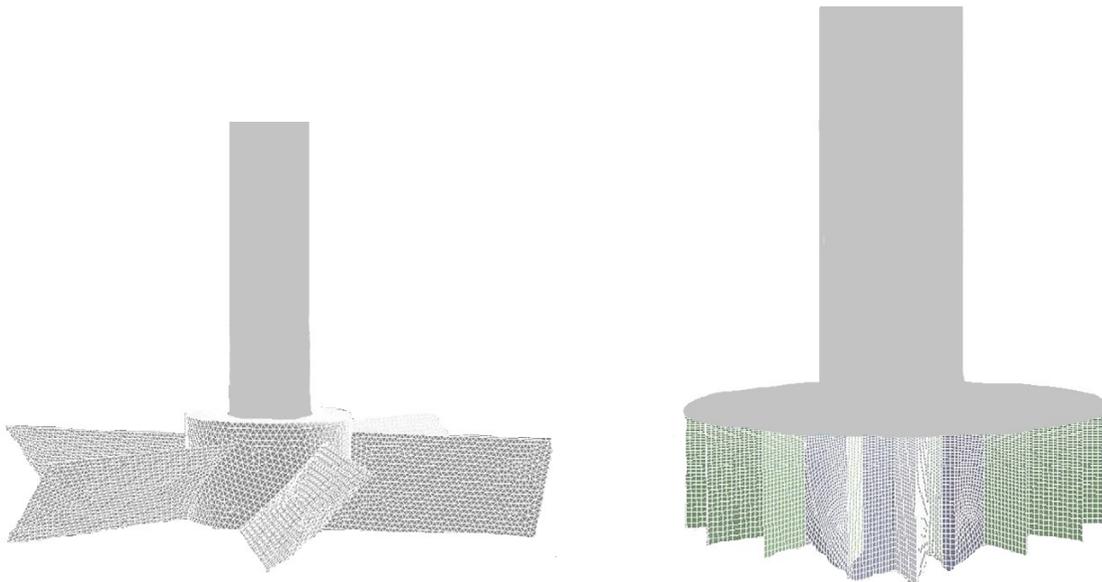
Figure 1.5 a) Pitch blade turbine (PBT- left) 270000   b) Flotation cell impeller 652000CV (right) redrawn from [17]
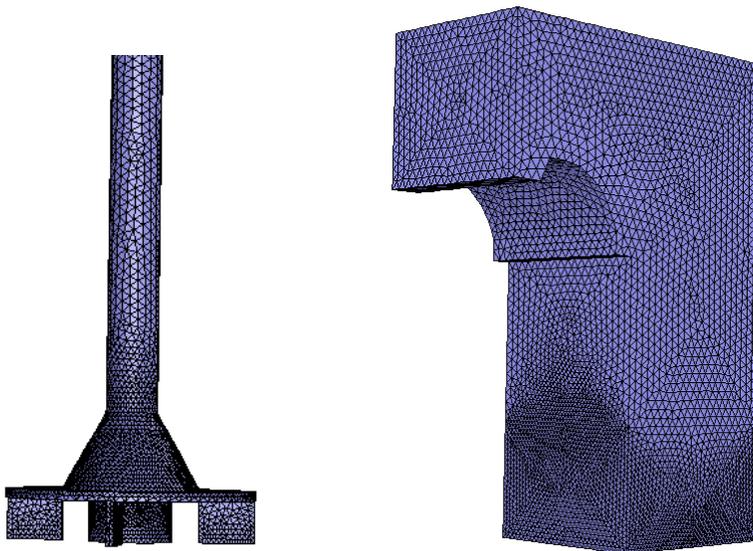
Figure 1.6 a) Impeller in a flotation cell designed by us (left) b) Flotation cell model outlet view

A pilot scale mechanical flotation cell containing non-Newtonian Bindura nickel slurry was then modelled. The predicted flow in the flotation cell was also experimentally validated by using piezoelectric pressure sensors to identify the cavern boundary in the flotation cell. It was possible to accurately predict both the shape and size of the cavern formed by the pitch-blade turbine, and it was decided that the SST k-ωk-ω turbulence model was more suitable to model turbulence. It was also found to be most appropriate to use an iso-surface of viscosity equal to the yielding viscosity to define the cavern boundary, as long as the yielding viscosity was set high enough to make the cavern size independent of this value. When modelling the flotation cell, it was found that the non-Newtonian nature of the slurry produced considerably different flows when compared to water at the same impeller speeds, and this difference was amplified as the solid concentration increased. In the 60 wt. % slurry a cavern forms at the two lowest impeller speeds, with the majority of the flow localized into the region below the stator disc, and the area of moving fluid above the disc reduced due the yield stress. The size of the cavern was found to be inversely proportional to the yield stress and viscosity, i.e. the ore type and solids concentration of the slurry, but further research needs to be conducted to find the effect of each variable individually. The predicted cavern sizes were also successfully validated experimentally. In conclusion, the findings presented in this paper indicate that the rheology of mineral slurries is affected by their solid concentrations, which therefore has an impact on flotation cell hydrodynamics.

Flotation modelling to date has concentrated either on macro scale processes or on ideal micro scale processes, there has been no attempt to integrate detailed models at different scales. Bubble particle collision efficiency with mobile bubble surfaces in a turbulent flow is investigated from a multi scale modelling viewpoint and a general methodology for modelling is present. Comparisons

were carried out to illustrate the method. Turbulence effects on bubble-particle collision efficiency were systematically studied using a 3D k–ε turbulence model.

One other work describes how to use a CFD numerical simulation with Lagrangian particle tracking model to calculate bubble-particle collision efficiency in a turbulent environment [19]. The bubble-particle collision efficiencies with large particle Stokes number, mobile bubble surface and in a 3D isotropic turbulent flow were calculated firstly. By comparing the computed results with experimental data from the literature, the CFD simulation was shown to be a successful tool that correctly predicts the bubble-particle collision efficiency in a quiescent environment. The CFD method was then applied to the investigation of bubble-particle collision efficiency in a turbulent flow. The bubble and particle motions in turbulent flotation cells are more complicated. The bubble-particle collision efficiency is influenced by the turbulence in two ways: firstly the turbulence effects on local average bubble-slurry relative velocity, and secondly turbulent dispersion of particles. The two mechanisms whereby turbulence affects bubble-particle collision efficiency were quantitatively analyzed. A stochastic model was used to produce a fluctuating flow field and the flow was employed to calculate particle trajectories using a Lagrangian tracking approach. The simulation results of bubble-particle collision efficiency in a quiescent environment are quantitatively consistent. Further direct numerical simulations of bubble-particle collision efficiency in a turbulent flow and bubble motion phenomenon in a turbulent flow were analyzed. This study indicates that a micro scale simulation of bubble and particle behaviors, coupled to macro scale CFD simulations of flotation cells, provides a powerful tool predicting the flotation rate in a real flotation cell.

Simulation of single and two-phase flow in a pilot DAF tank were presented [20]. Implications of numerical model of a DAF tank in the absence of third dimension were investigated. Based on the

results it was confirmed that applying a 2D model is not sufficient to predict the flow in the contact zone. Two-phase flow in the separation zone can be predicted to some extent by using 2D model. The simulations demonstrated that there was not much reduction in the magnitude of the velocities in 3D model compared to 2D model. However, the anticipated 3D-floweffects (velocities in the y-direction) are indeed observed in the simulations. Two-phase numerical simulations by a 3D model demonstrate that the stratified flow pattern in the separation zone can be performed successfully. The sensitivity of 3D model to the distribution of the air and water from the needle valves was presented. The latter effect influences the stability of the solution and its effects can be alleviated by the using a transient solver. Finally, this study indicates validation of a numerical DAF model with experimental measurements is an extremely cautious task. If there are considerable changes in flow pattern over time and velocity measurements are made separately, then the different measuring points are not really considered simultaneous and not correlated to each other. Consequently, the experimentally measured flow pattern will unlikely to reproduce by using the numerical simulations

A three-dimensional CFD model combined with the rheological properties of sludge was developed to quantify mixing parameters in a full-scale anaerobic digester [21]. The results were found to be consistent with measured experimental tracer response curve. A new parameter, which was called UI (uniformity index), was defined to predict the mixing dynamics. The dynamic variation in the UI was related to the visual patterns of tracer mixing. This model allowed to determine optimum mixing time while presence of different solid concentration in a full-scale digester.

The key components of flotation cells which are known as motor-stator mechanisms serve to mix the slurry and the air bubbles. The energy consumption and efficiency of a flotation cell can be

improved by optimization technique of rotor-stator mechanism. Firstly, the angle of the impeller blades, which needs special design consideration of rotor-stator mechanism, is key part for the pumping and power consumption of a flotation cell. The combination of PIV measurements and CFD simulation was employed to investigate flow pattern of a flotation cell with different impellers. Results from PIV and CFD also revealed the flow characteristics of the test cross-section area under the impeller. It was found that the PIV measurements were in good agreement with the CFD prediction results, and interestingly the backward, radial and forward impeller produce very identical flow patterns with upper and lower circulations. The impeller circulation volume can be estimated by a velocity-area method which integrates the axial velocity in the area of the selected section using CFD simulation. The circulation volumes of the backward impeller and radial impeller were found to be equal and are approximately 7% greater than that of the forward impeller. Thus, the backward and radial impeller are preferable when large-volume circulation is required [22]. Based on the CFD simulation, backward impeller is very efficient in terms of the power consumption which is 13% less than that of the radial impeller and 19% less than that of the forward impeller. The operation cost for the concentrator can be greatly saved by installing the backward impeller. This study is very helpful for the structural design of impellers for KYF flotation cells.

The effects of grid resolution and discretization scheme on the CFD simulation of fluid flow in an impeller stirred tank using the MRF impeller rotation model and the standard k–e turbulence model were investigated [23]. The CFD model predictions have been compared with the experimental data. The accuracy of the CFD model has been evaluated in terms of the predicted flow field, power number, mean velocity components and the turbulent kinetic energy. From these results one may conclude that:

Flow field: The general flow field patterns can be predicted using relatively coarse grids but predicting subtler phenomena in the flow field, such as the formation of trailing vortices, requires very fine grids.

Power number: The accuracy of the power number prediction is strongly dependent on the grid resolution and the discretization scheme. It seems plausible to predict the power number accurately by using very fine grids and high-order discretization schemes.

Mean velocity: The accuracy of the mean fluid velocity predictions is not strongly influenced by the grid resolution or discretization scheme. The accuracy of the turbulent kinetic energy predictions is dependent on the grid resolution and the discretization scheme which indicating very fine grids and high-order discretization schemes required to avoid large discrepancies in CFD predictions. A grid consisting of nearly 2 million control volumes in one half of a 15 cm diameter stirred tank with a combination of high-order discretization scheme, was needed for more precise prediction of the turbulent kinetic energy. These results suggest that the poor predictions of turbulence obtained using the k–e turbulence model which is often noted in the literature may be due to possible numerical errors rather than deficiency of the turbulence model.

A Computational Fluid Dynamics (CFD) model for the prediction of the flotation rate constant in in a flotation tank with a Rushton turbine was built [24]. The main assumption for the model development was a first order rate kinetic of the flotation process. An Eulerian–Eulerian framework combined with the dispersed k–ε turbulence model was supplemented with user defined functions to implement the local values of the turbulent flow into a kinetic model. Simulations were performed for quartz at different operational conditions. The numerical predictions were confirmed with experimental data and analytical computations using the fundamental flotation model. The results showed that the CFD-based model successfully produced

the trend of experiments for a range of particle sizes and also yielded improvements in the predictions of flotation rate constant compared with the theoretical calculations. It was concluded that the developed CFD model is able to predict the flotation rate constants of the floating quartz with different hydrophobicity, agitation speed and gas flow rates with lower root mean square deviation [25].

Collision behavior of a smaller particle into a larger stationary droplet which is considered as very important phenomenon related to many process engineering applications and was investigated [26]. The collision process was studied experimentally by using high speed video imaging involving glass ballotini particles (diameter: 1.13 ± 0.02 mm) and a supported stationary water droplet (diameter 3.41 ± 0.01 mm) at different particle impact velocities (Weber number range: 0.2–13.5). It was observed that a transition occurs from partial to complete penetration with a decrease in sinking time and significant shape deformation of the droplet happens when Weber number was increased. One dimensional transient force balance approach was adopted which is the combination of six major forces including: gravity, capillary, fluid drag, buoyancy, pressure and added mass to model penetration process numerically. It was found that the capillary force controlled the interaction process. Due to awareness of the limitation of the one dimensional model for the details of the collision physics especially the movement of three phase contact line (TPCL) on the particle surface, a 3D computational fluid dynamics (CFD) model was developed using the multiphase volume of fluid (VOF) method combined with the dynamic meshing technique. The CFD model was supported by experimental measurements of the sinking time of the particle and collision dynamics including shape deformation of the droplet.

The optimal location of impellers was obtained by using Evolutionary Programming and CFD techniques [27]. The location was evaluated by the determination of mixing time and power

consumption. ANSYS Fluent were used for calculations and number of elements are 270 000. Tank configuration was L= 0.287m H= 0.45m and impeller diameter D= 0.15m, width of impeller W= 0.038m. Angular velocity of 100 rpm was used during the mixing process. The system H is the optimal one-impeller system, while the optimal two-impeller system is defined as P. In the evolution process the best individuals are selected according to the operators: selection and mutation. This approach represents an efficient method for optimizing the mixing process in stirred tanks

Rotation speed	Sizes of the cell (m)	Size of impeller m	Software used	N of grid points	Author&year of the article
50 rpm	D=0.445	D=0.2286 m	Gridpro, Gambit	3.1 million	Acharya 2012
100 rpm	D=0.287 H=0.45	D=0.15 W=0.038	ANSYS Fluent	250 000	Alfaro 2015
10-190 rpm	D=0.40	D=0.18	Fluent	144 031	Chan 2008
68-367 rpm	D=0.54 H=0.445	D=0.15 W=0.10	Fluent	260 000	Delgon 2009
269 rpm	D=0.45	D=0.254	ANSYS CFX	270 000	Gerber 2015

Table 1.1. Modelling characteristics of flotation cell from different papers

CFD model of sewage sludge mixing in anaerobic digesters was developed [28]. In this study digestion was conducted in 6l cylindrical vessels which were continuously stirred by various speed 20-200 rpm. Fluent v6.3.26 was used for simulation. Five turbulence models; standard k-ε (Sk-ε), Realizable k-ε (Rk-ε), Renormalized k-ε (RNG k-ε), Standard k-ω (Sk-ω) and Reynolds Stress Model (RSM) were assessed. For all simulations the residuals were set as $1*10^{-5}$. Three meshes were constructed containing 278183, 316704 and 1608169 cells. The effects of increasing solids content of sewage sludge on the mixing characteristics of a laboratory-scale anaerobic digester are significant, and can be demonstrated in terms of velocity magnitude and volume of stagnant zones. The relationship between solids content and stagnant volume can be described effectively by a second order polynomial function. Laboratory scale biogas yield was neither impaired nor

improved by changes in mixing speed. Biogas yield can be maintained at velocity gradient values significantly below those recommended in the literature.

CFD modelling of non-Newtonian slurry in mechanical floatation was provided by using Herchel-Bulkey model with constants derived from experimentally determined slurry containing fibrous type material, serpentine.

A fully three-dimensional mesh was used to model half the PBT tank geometry, utilizing the symmetry of the tank to reduce computational cost. Periodic boundary conditions were applied to the cut planes. The mesh used to model the PBT consisted of a hybrid tetrahedral/quadrilateral mesh of approximately 270000 cells.

The working fluid was represented as a single phase liquid of using the Herschel–Bulkley non-Newtonian model included in Fluent. As well as laminar simulations, two different RANS turbulence models were investigated in this study, the standard k-ε and shear stress transport (SST) k-ω models. The latter model combines the Wilcox k-ω turbulence model and the standard k-ε model by using a blending function that activates the k-ω model in the near wall region, and the k-ε model away from the walls.

CFD simulations were conducted in order to investigate the effects of non-Newtonian mineral slurry rheology on the hydrodynamics inside a mechanical flotation cell [29]. It was possible to accurately predict both the shape and size of the cavern formed by the pitch-blade turbine, and it was decided that the SST k-ω turbulence model was more suitable to model turbulence. The modelling methodology used was first validated by modelling a pitch-blade turbine agitated tank and comparing results against published experimental cavern measurements. A pilot scale mechanical flotation cell containing non-Newtonian Bindura nickel slurry was then modelled. The predicted flow in the flotation cell was also experimentally validated by using piezoelectric

pressure sensors to identify the cavern boundary in the flotation cell. The rheology of mineral slurries is affected by their solid concentrations, which therefore has an impact on flotation cell hydrodynamics.

Experimental and computational analysis of the impeller angle in a flotation cell by Particle Image Velocimetry (PIV) and CFD modelling was provided [30]. Rotor-stator mechanisms, which are the key components in flotation cells, serve to mix the slurry and the air bubbles. The optimization of rotor–stator mechanisms improves the metallurgical performance and decreases the energy consumption of a flotation cell. The angle of the impeller blades, which is an important aspect of the design of rotor–stator mechanisms, significantly impacts the pumping and power consumption of a flotation cell. The study was conducted on a 0.2 m3 air-forced laboratory KYF flotation cell. The structure was designed based on a laboratory KYF flotation cell. The characteristics of laboratory KYF flotation cells are similar to those of industrial KYF flotation cells. The flotation cell consisted of a tank with an inner diameter of 700 mm and liquid surface height of 630 mm. The impeller consisted of six blades with a diameter of 220 mm, and the stator consisted of sixteen blades with a diameter of 350 mm.

CFD simulations were implemented using computational fluid dynamics code CFX 14.0 by using a standard k–ε turbulence model. The residual RMS of each equation was less than 1×10^{-4}. For an impeller rotating in a flotation cell, the model needs to be divided into multiple zones that are separated by interface boundaries. One zone involves moving a component impeller and the other involves the stationary components, the tank and stator. The Multiple Reference Frame (MRF) model is the simplest approach for analyzing multiple zones. The circulation volume of the backward impeller is similar to that of the radial impeller and is larger than that of the forward impeller by approximately 7%. In other words, the backward impeller and radial impeller would

be a better choice when a large circulation volume is needed. The power consumption of the backward impeller is 13% and 19% lower than that of the radial impeller and forward impeller, respectively. The backward impeller was demonstrated to be advantageous because it saved energy compared with the other two impellers.

Section 1.5 CFD simulations of bubble columns

Study of bubble-induced, gas–liquid multiphase flow in bubble columns is important for the product development, design and scale-up of many industrial process devices such as bubble column reactors, and understanding flotation cells, boilers. Investigation of bubble generation and dynamics has an important role in modelling of flotation cell. The classical flat bubble column is investigated using the methodology of Large Eddy Simulation in conjunction with two-way coupled Lagrangian particle tracking technique [31]. A concept named PSI-ball (particle-source in ball) is formulated to map a Lagrangian quantity to the Eulerian reference frame. Good prediction accuracy was achieved in comparison with experimental data such as flow and transition bubble dispersion patterns.

In other study two-phase flow in 2d and 3d coordinates were modeled by using of Navier-Stokes equations with Eulerian representation [32]. The comparison of Upwind and TVD discretization schemes were provided for solving gas phase equations. As a result it was shown that TVD scheme with Eulerian/Eulerian method as well as Eulerian/Lagrangian method show a good agreement. In case of UPWIND scheme, due to influence of numerical diffusion, the agreement was not obtained. In order to decrease numerical diffusion in case of UPWIND method of solution finer grid could be used. Eulerian/Lagrangian methods as well as TVD were not affected by numerical diffusion.

In case when gas hold up was more than 10% none of the methods described above was accurate, since bubble-bubble interaction must be taken into account.

In different work of the same authors two and three dimensional simulation by using standard k-ε model is provided in aerated flat bubble in laminar and turbulent cases. In these cases it was shown that 2D simulation has a strong influence on the numerical solution. In the case of 2D laminar model the results depend on the space resolution, finer space grid gives more vortices according to turbulent character of the flow. From other hand for 2D k-ε the value of the effective viscosity was overestimated by one magnitude, which affects the transient character of the flow. In comparison with 2D model 3D k-ε model showed a good agreement with experimental results [33]. The validation of the results was presented on the second part of the work of the same authors by using flat bubble column with rectangular cross-section. The liquid level of the 50 cm showed steady-state behavior, but higher liquid level showed transient flow [34]. The qualitative validation of simulation was made by use of video images obtained from the tank. It was shown that 3d k-ε model shows good agreement with experimental results.

Section 1.6 Simulation of single bubble dynamics

In literature first bubble model corresponds to one of the greatest engineers, scientists and artists of, Leonardo Da Vinci in 15th century. Images from his notebook say that Da Vinci was interested with air bubble in water model which indicates to the importance and oldness of the problem. Da Vinci explained sinusoidal movement of air bubble from underneath of water with the dynamics of the air and with attempt of bubble to mix with the atmosphere.
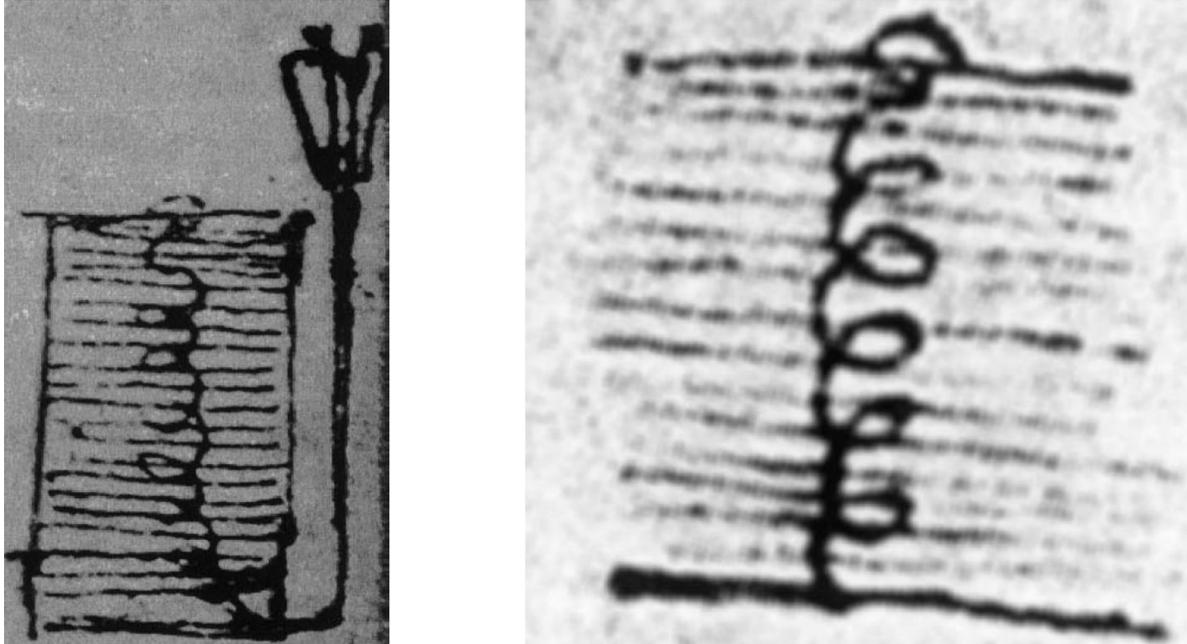
Figure1.7 Images of helically rising air bubble from Leonardo Da Vinci's notebook [35]

Bubbles in a liquid phase are come across very different industrial (flotation and bubble column reactors) and natural processes. In this view it is important to understand behavior of bubbles in a liquid phase. There have been done numerous CFD works related to air bubble growth and dynamics in literature.

Gas holdup and single bubble velocity profile were measured in two different systems: F150 and 1-pentanol [36]. At equal concentrations it was shown that bubbles in 1-pentanol rise more slowly than in F150 solution. Lower gas holdup achieved in 1-pentanol. In NaCl solution bubbles rise more quickly than in MIBC, which corresponds to lower gas holdup in case of NaCl solution. In flotation process gas holdup measurement and applications has their importance.

 Multi-phase flows where sharp interfaces are introduced are encountered in a variety of industrial processes. There is a need to track the interface separating the fluids. In this view 3D VOF method is used to feature an interface reconstruction technique dependent on piecewise linear

representation [37]. It was shown that computed terminal rise velocities were not affected by the size of the computational domain. Data taken from bubble diagram of Grace were agreed with the size and shapes of isolated gas bubbles rising in quiescent fluids. The model was applied for coalescence of two bubbles rising in viscous liquid.

In different work of similar authors a three dimensional Front Tracking method and two dimensional Volume of Fluid method were used to analyze the closures for the drag and virtual mass forces that effect on single air bubble rising in quiescent water system [38]. Because of increasing importance of the surface tension forces in bubbles smaller than 3mm sharp reduction of drag coefficient were observed. Computed bubble terminal rise velocities were higher compared to experimental data, which can be also explained by small impurities that can be available in water.

Simulation of the rising bubble in a viscous liquid was conducted by front tracking method with modelling of two-phase fluid systems [39]. Velocity field was solved by using finite volume method based on SIMPLE algorithm. Non-dimensional parameters such as Reynolds number, Bond number and viscosity, density ratios were used to study bubble shapes and velocity in a wide flow regime. Effect of viscosity and density ratios between two fluids on bubble shape were analyzed.

Effect of surfactant on the dynamics of a crude oil droplets ranging 3 to 8.5 mm in water column was studied [40] by using of CFD modelling in ANSYS Fluent software and validated experimentally. Range of oil droplets were created by using nozzles with different diameters. Behaviors of crude oil droplets were analyzed in systems with different surfactant (SDS) concentrations varied from 0-750 ppm.

26

Rise velocity profile and terminal velocity of single bubbles with <2mm sizes as a function of temperature in two different surfactant solutions of water were investigated [41]. Surfactants or frothers used in industry by flotation process like Triton X-100 and Downfroth 250 were used. Without surfactant bubble reaches maximum velocity after some point. With surfactant the velocities of the bubbles decrease and reach constant after some point which is identified as transient velocity.
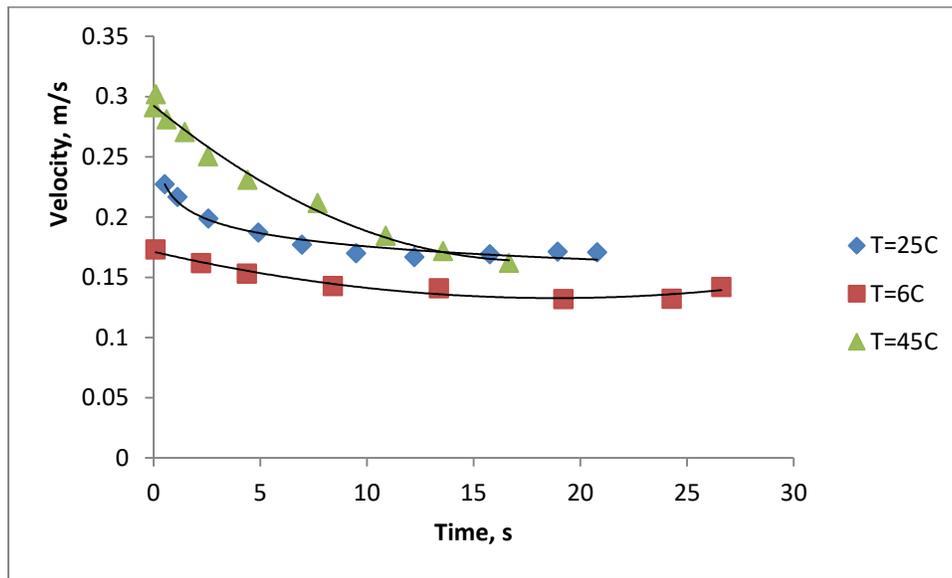
Figure 1.8 Velocity profile of air bubble with 0.8 mm diameter in tap water at different temperatures [41]

As it is seen from velocity profile of bubble in tap water, the velocity is decreased after some time which can be explained by impurities in tap water. These impurities sit on bubble boundaries and increase drag force which results by decrease of bubble velocity. Bubble deceleration happens to be more at high temperatures compared to low temperature.

The dynamics of bubble rise smaller than 1 mm size and the impact of solid surfaces on bubbles were studied [42].

Chapter 2 Numerical Modelling of Air Bubble Dynamics in Water

Section 2.1 Analysis of a single bubble modelling

After studying some models successfully implemented in literature we decided to point our focus to bubble generation and study of the air bubble dynamics in water. Some good works including Albadawi et all [43] were done and part of the results obtained in our simulations are compared to the experimental data extracted from the paper above. Basic models use multiphase models which cannot predict single bubble behavior. In this view it would be interesting to study the influence of orifice diameter, surface tension on the bubble dynamics in order to understand the interaction of different parameters on flotation cell.

We have attempted to simulate the generation of single gas bubble in a liquid using the volume-of-fluid (VOF) technique, which allows us to describe the complex bubble dynamics using the fluid phase properties as inputs.

The VOF model resolves the transient motion of the gas and liquid phases using the Navier–Stokes equations, and accounts for the topology changes of the gas–liquid interface induced by the relative motion between the dispersed gas bubble and the surrounding liquid. The finite-difference VOF model uses a donor–acceptor algorithm to obtain and maintain an accurate and sharp representation of the gas–liquid interface. The VOF method defines a fractional volume or 'color' function $c(x, t)$, which is a function of position vector x and time, t. The color function indicates the fraction of the computational cell that is filled with liquid, and varies between 0, if the cell is completely occupied by gas, and 1, if it consists only of liquid. The location of the bubble interface is tracked in time by solving a balance equation for this function [44].

In the literature characteristic of bubble growth and detachment was modelled by using Volume of Fluid and Level Set methods in ANSYS Fluent Software [43]. This paper was used for getting flow parameters and also a concept of modelling was done successfully and validated by experimental data. That's why this article was used for validation our CFD experiments on ANSYS Fluent. Experimental data's extracted from the paper were compared to bubble size obtained from our simulation. Then it would be to give brief review about the experimental setup of the facility used in the works of authors. It is a square glass tank with 50 mm filled with 20mm of water in it. Bubbles are generated by stainless steel orifice with 1.6 mm diameter. Gas flow rate is controlled by 2.5ml syringe infusion pump. High speed digital camera with frame rate of 1000 Hz and with an exposure time of 0.5 ms was used. Bubbles were illuminated by 6 of 300 lm LED bulbs in array. Ultra clean water with specific resistance of 18.2 MΩ was used.

Liquid Density	998.2	kg/m^3
Liquid Viscosity	0.001	kg/m^3
Gas density	1.225	Kg/m^3
Gas viscosity	$1.79*10^{-5}$	Kg/ms
Surface tension	0.073	N/m
Gravity	9.81	m/s^2
Orifice radius	0.8, 0.4	Mm
Flow rate	150	Mlph

Table2.1 Fluids physical properties

Boundaries of the bubble were detected by using of custom code generated by the authors. Uncertainty of the conversion and detection was 1 pixel or ±0.0134 mm. The simulation is conducted by using axi-symmetrical domain with orifice radius of 0.8 mm. The mesh step size of $\Delta x = 1*10^{-4}$ m is chosen so that, the orifice diameter is modelled by using 16 cells. Time step $\Delta t =$

$1*10^{-5}$s is chosen. At the lower wall, a static contact angle is assumed as θs= 20°. Physical

properties of the fluids are introduced in table 2.1.

Section 2.2 Model Formulation

In VOF method some mass conservation, volume fraction continuity equation and momentum

equation for immiscible two phases are solved. The equations are given below.

Mass conservation equation:

$$\frac{\partial \rho}{\partial t} + \nabla(\rho \vec{u}) = 0 \tag{2.1}$$

Volume fraction continuity equation:

$$\frac{\partial \varepsilon}{\partial t} + u \cdot \nabla \varepsilon = 0$$

$$(2.2)$$

Momentum equation for immiscible two phases:

$$\frac{\partial}{\partial t}(\rho \vec{v}) + \nabla \cdot (\rho \vec{v} \vec{v}) = -\nabla p + \nabla[\mu(\nabla \vec{v} + \nabla \vec{v}^{T})] + \rho \vec{g} + F \tag{2.3}$$

Volumetric surface tension force F represented in momentum equation can be expressed in terms

of pressure change across the surface. The force at the surface can be expressed as a volume force

and added as a source term to momentum equation. In the presence of two phases the equation for

surface tension force can be written as:

$$F = \sigma_{ij} \frac{\rho k_i \nabla \alpha_i}{\frac{1}{2}(\rho_i + \rho_j)} \tag{2.4}$$

In simulation process change of the density for every grid is calculated and updated for every calculation. The change of mixture density is calculated by fraction of gas or liquid phase for every grid by equation:

$$\rho = \rho_g \cdot \varepsilon + (1 - \varepsilon) \cdot \rho_l \qquad (2.5)$$

For simulation two different domains were created with 80000 and 160000 CV. Domain 1 has a nozzle diameter of 0.8 mm, domain is designed with smaller nozzle diameter. For accuracy of the simulations in the second case with smaller air inlet orifice more control volumes were used.
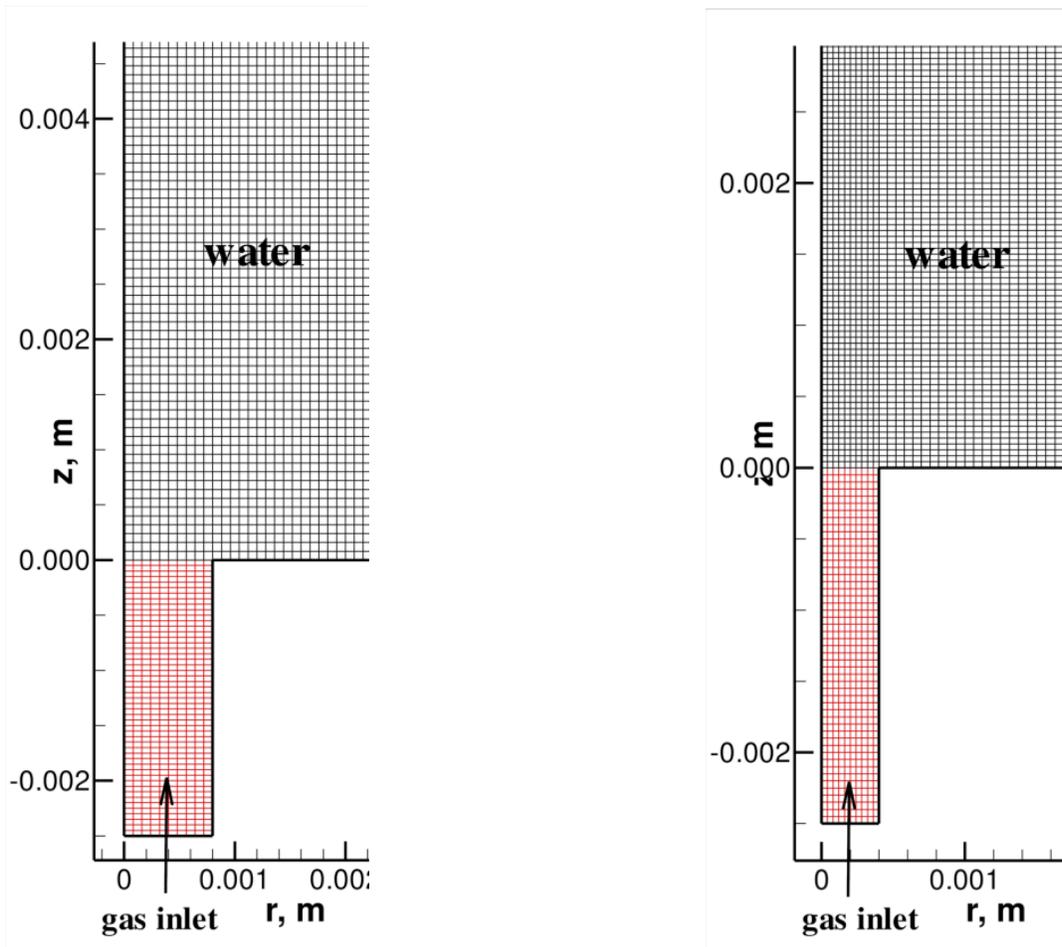
Figure 2.1 Size and zoomed view of inlet section, left: Domain 1 with grid size 80000 CV, right: Domain 2 with grid size 160000

In case of smaller orifice twice as much grid size was used for accuracy of calculations. In VOF model accuracy is decreases when interface length scale gets closer to computational grid. That's why it is important to have larger number of grid points in case of smaller orifice. The VOF model would not be applicable in case when interface length scale smaller than grid points. By having enough control volumes and accurate equations, VOF model is robust and accurate. In calculations one set of momentum equations are solved for all fluids in the system.

Section 2.2.1 Boundary conditions

On side we defined stationary wall boundary condition with no slip. Wall adhesion contact angle between phases is constant 20 degree. Air inlet was defined from the bottom of the tank. For velocity specification method magnitude normal to boundary were chosen. On the top of the tank pressure outlet type of boundary condition was used. Operating pressure is defined as 101325 Pa and operating density is 1.225 kg/m^3. In tube zone also boundary conditions were identified as stationary wall with no slip wall adhesion contact angle is 90 degree.

 Numerical modelling of air bubble dynamics in water was modelled based on numeric described below:

Grids: Geometry1: 80000 CV; Geometry2: 160000 CV

Spatial Discretization: Momentum: QUICK,

Volume Fraction: Geo-Reconstruct scheme (explicit)

Pressure-Velocity coupling: PISO

Time step: $2*10^{-5}$ s

Number of iterations per time step: 35

Min Residual: continuity 10^{-14}; momentum equation 10^{-10}

Geometry one has a nozzle diameter twice as large as compared to the Geometry two, that's a main reason for a need of better accuracy. Control volume is a mathematical abstraction used to create models of physical processes. QUICK refers to Quadratic Upstream Interpolation for Convective Kinematics is a differentiating three point upstream scheme. QUICK scheme is a third order accuracy and used to solve convection-diffusion equations. Pressure velocity coupling was provided by PISO (Pressure implicit with separating operator) algorithm. It is a pressure velocity algorithm used to solve Navier Stokes equation.

Also there are some assumptions made by modelling of the system with axisymmetric domains. For lower Reynolds numbers with laminar systems, generation of the small bubbles can be modelled by axi-symmetrical domains assuming the rise to be linear and symmetrical. In the turbulence systems with bigger Reynolds number, it is more accurate if the rise of the bubble modelled 3D. But 3D modelling takes more time and computationally is expensive. In this view we have assumed the system to be symmetric and provide our calculations based on these assumptions.

Section 2.3 Results of simulation

On the first run we simulated the bubble formation in geometry 1 with given conditions above. The results of the simulation are described in figure 2.2. As it is seen from the figure bubble detachment occurs at the beginning of the second sec. Bubbles generated on the first run tend to be spherical at the beginning but change to ellipsoidal after some time.
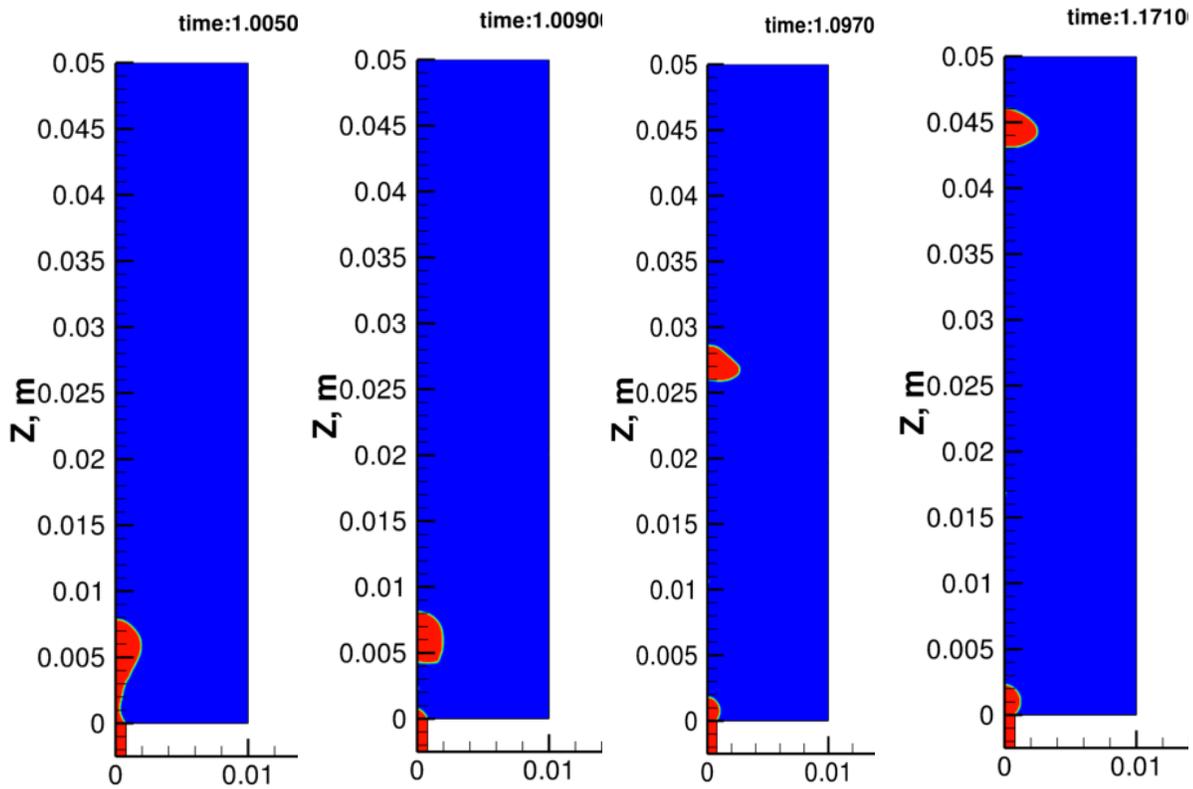
Figure 2.2 Results of simulation Geometry 0.8 mm nozzle radius, air inlet velocity 150 mlph, surface tension: 72.8 mN/m

The results of the first run with geometry of 80000 control volumes and 0.8 mm nozzle diameter

is described in figure 2.2. As it is seen from the first picture bubble detachment time is 1.005 s and

high surface tension deforms bubble after detachment.
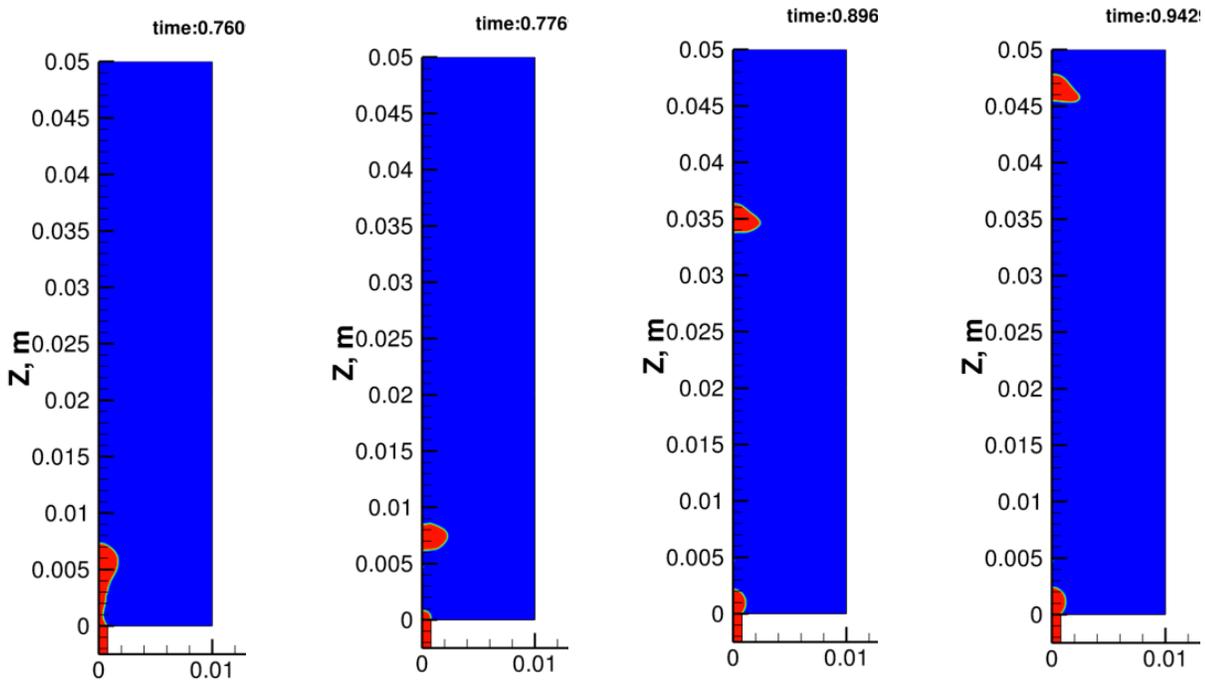
Figure2.3. Results of simulation Geometry 80000 CV, nozzle radius: 0.8 mm, air inlet velocity: 150 mlph, surface tension: 50 mN/m

Later simulation of the bubble dynamics with lower surface tension has shown that surface tension has an effect on bubble size. Smaller surface tension leads to smaller bubble size and in this case detachment time is lower. Lower detachment time is also observed in the cases where air inlet velocity is higher. Surface tension effect also the shape of the bubble. In the cases with higher surface tensions bigger bubbles are formed. Bubble is more spherical at the beginning after detachment and tends to be more ellipsoidal after rise.
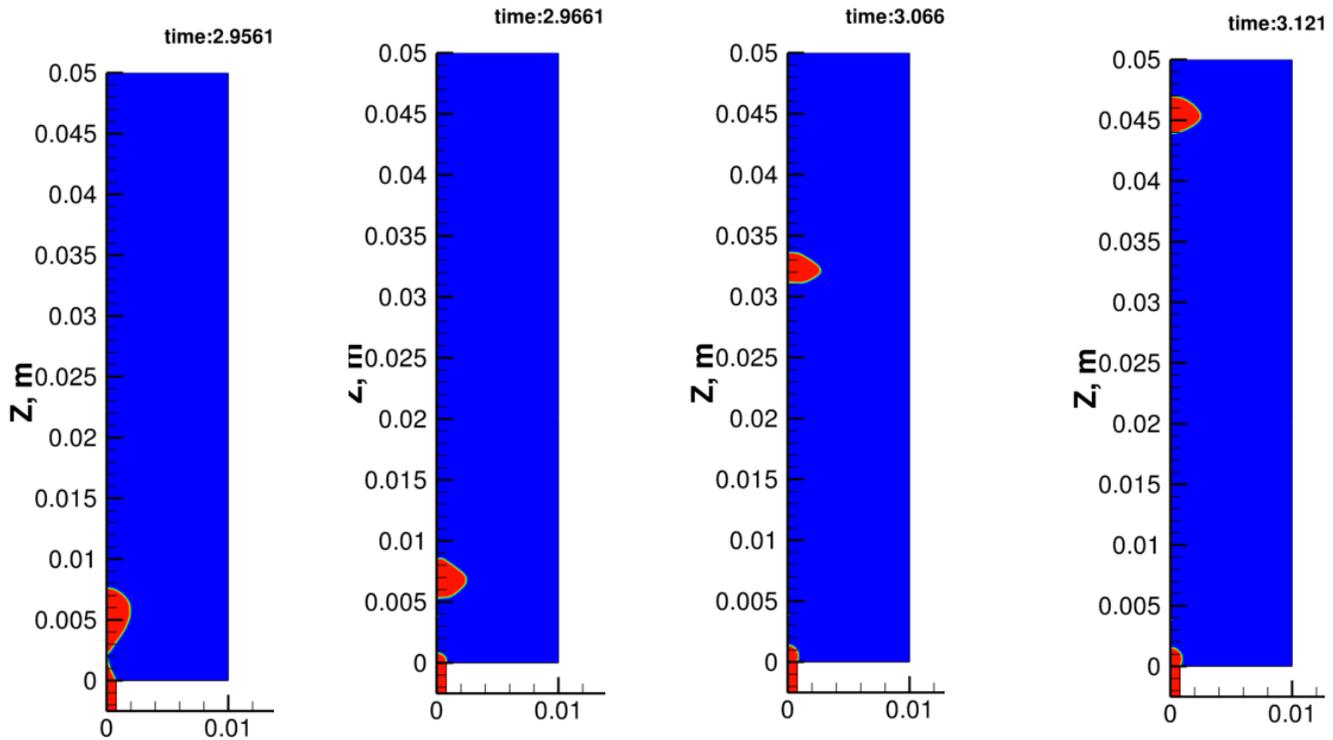
Figure 2.4: Results of simulation Geometry 80000 CV, nozzle radius: 0.8 mm, air inlet velocity: 50 mlph, surface tension: 72.8 mN/m

Then we have decreased air inlet velocity by three times in order to understand bubble behavior. As it is seen from the comparison of the results in the case with lower air inlet velocity bubble size is bigger than the other cases with lower surface tension and similar to the case with higher air inlet velocity. So, it can be concluded that the air inlet velocity does not affect much the bubble size and form. Later we lowered surface tension to 50 mN/m and calculated the bubble dynamics to see effect of the low surface tension and low air inlet velocity.
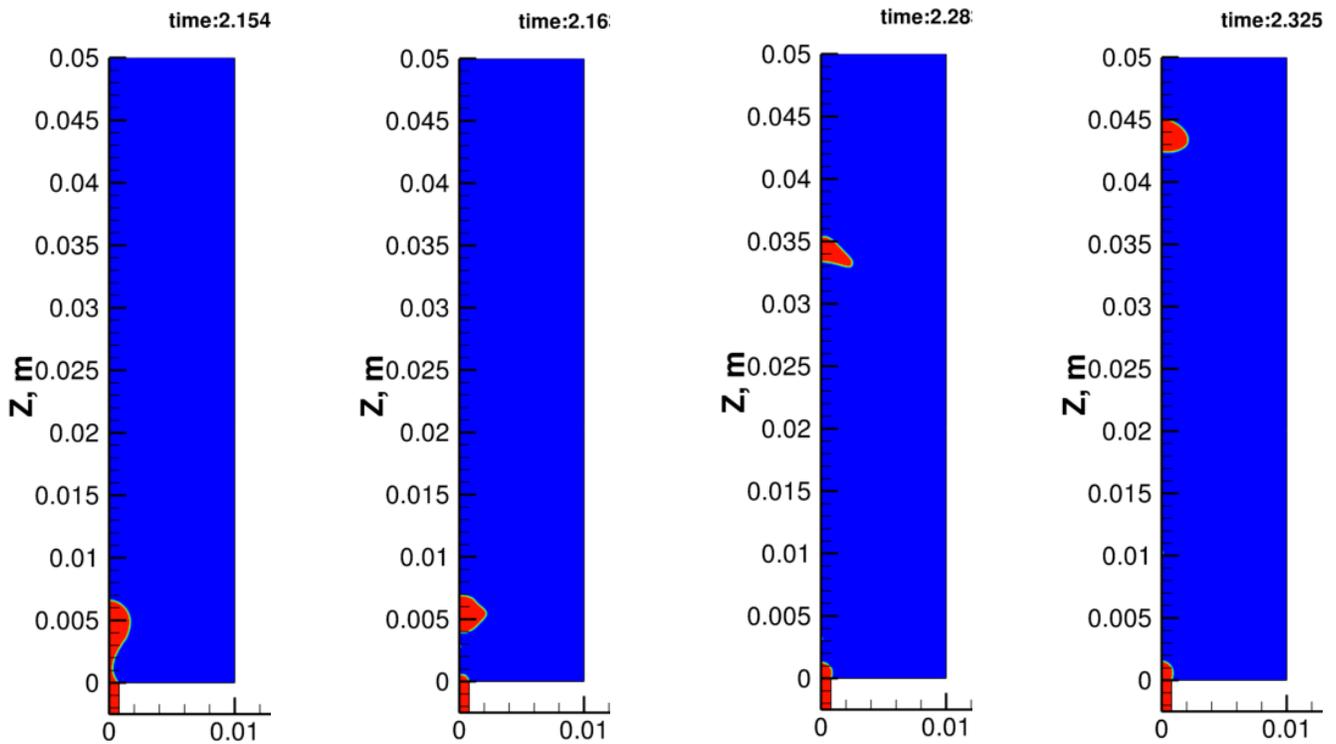
Figure 2.5 : Results of simulation Geometry 80000 CV, nozzle radius: 0.8 mm, air inlet velocity: 50 mlph, surface tension: 50 mN/m

As it is seen from the results in figure 9, decreasing surface tension and the velocity leads to smaller bubble size and less detachment time than in previous case.

As it is seen from industrial processes decreasing surface tension of the medium leads to smaller bubble size, thus can be achieved by either adding surfactants or decreasing the nozzle diameter of the air outlet. We have decreased the nozzle radius twice from 0.8 mm to 0.4 mm, to see effect of the nozzle size on bubble dynamics. In this case new geometry with 160000 control volumes was used. Increasing control volumes leads to more accurate results and in this case time step was twice as lower as the first case.
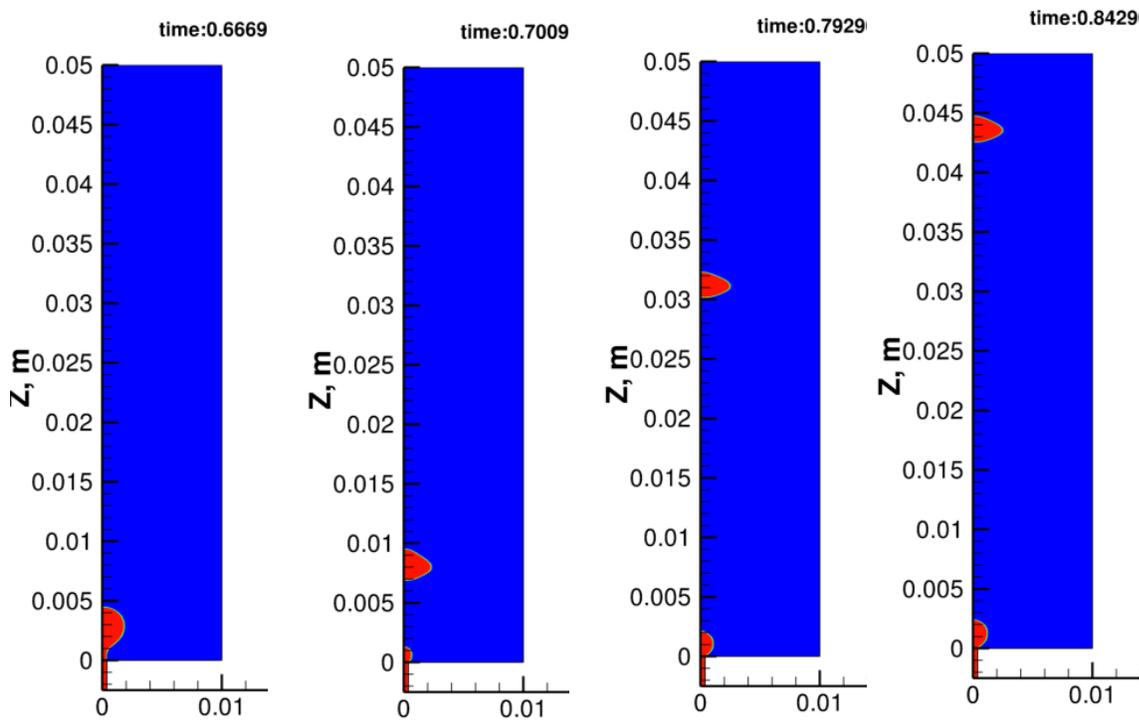
Figure 2.6 Results of simulation Geometry 160000 CV, nozzle radius: 0.4 mm, air inlet velocity: 150 mlph, surface tension: 72.8 mN/m
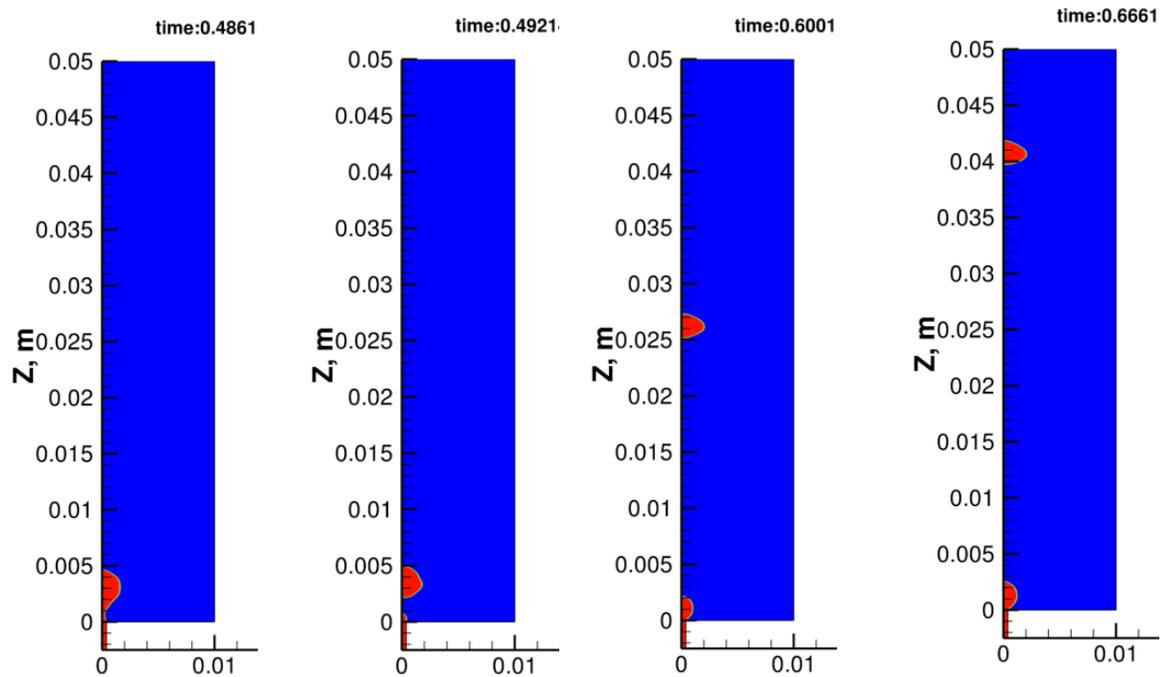
Figure 2.7 Results of simulation Geometry 160000 CV, nozzle radius: 0.4 mm, air inlet velocity: 150 mlph, surface tension: 50 mN/m

As it seen from the results of the simulation bubble size is decreased by decrease of surface tension value. Velocity of inlet air effects detachment time of the bubbles. The comparisons of the bubble detachment and rise for different nozzle diameter and surface tensions give us possibility to understand change of bubble dynamics depending on the system. In every case there have been observed that once bubble is detached from the nozzle some hold up time is needed before bubble starts to gain its transient velocity.
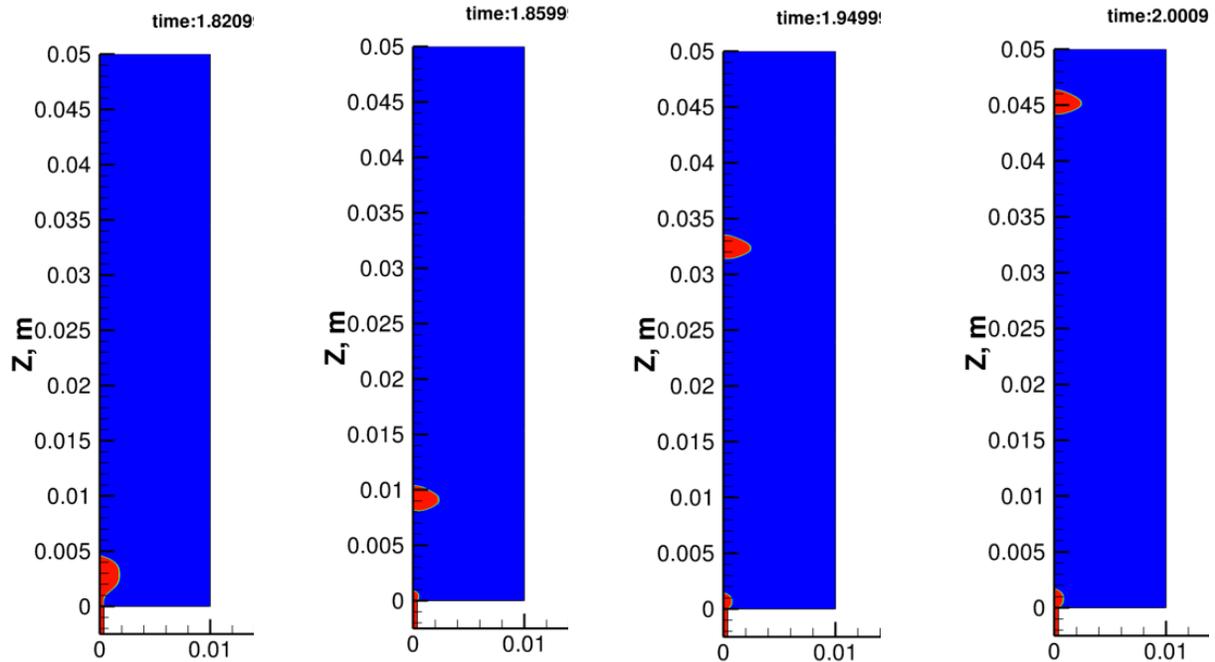
Figure 2.8 Results of simulation Geometry 160000 CV, nozzle radius: 0.4 mm, air inlet velocity: 50 mlph, surface tension: 72.8 mN/m

Comparisons of the bubble shapes depending of the different nozzle diameter give the possibility to understand how the bubble size changes once nozzle diameter decreased twice.

It is shown that twice decrease the air inlet path will 20 to 30 % change the size of the bubble depending of the surface tension. Also smaller bubbles are obtained by decrease of the surface tensions. These two parameters are the most important for flotation processes if smaller bubble sizes are desirable.
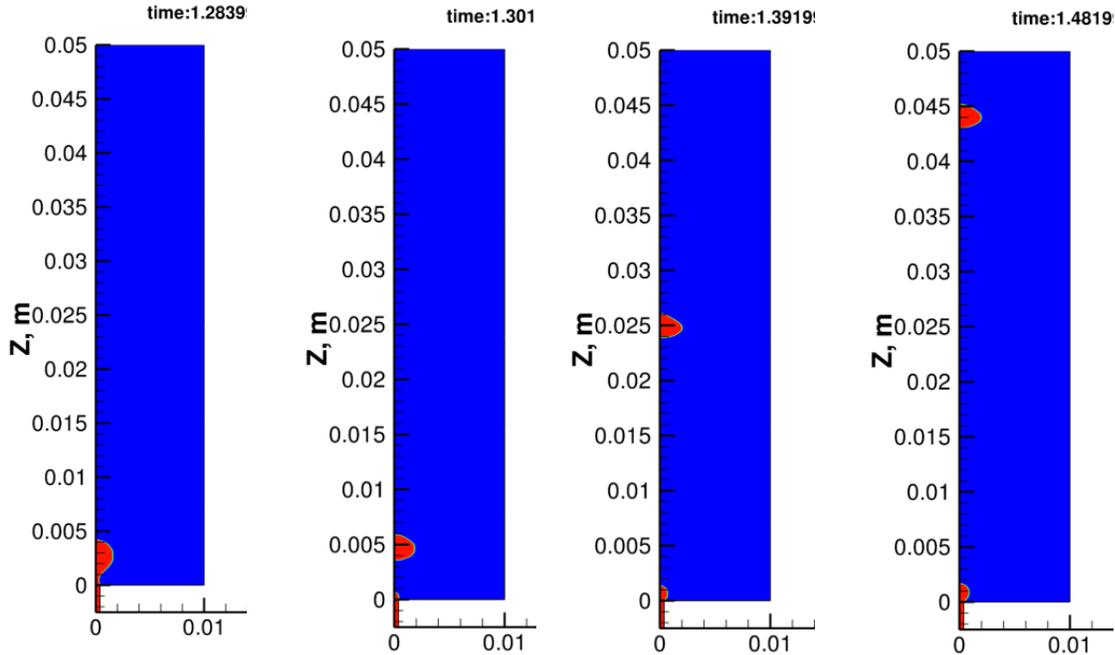
Figure 2.9 Results of simulation Geometry 160000 CV, nozzle radius: 0.4 mm, air inlet velocity: 50 mlph, surface tension: 50 mN/m.

The comparison of the results in second case with lower nozzle diameter shows that smaller nozzle diameter leads to smaller bubble size in general.

Surface tension mN/m	Air inlet velocity	Detachment time	Bubble rise velocity
Geometry 1 : Nozzle radius 0.8mm			
72.8mN/m	50 mlph	2.956 s	0.25 m/s
72.8 mN/m	150 mlph	1.005s	0.24 m/s
50 mN/m	50 mlph	2.154s	0.238 m/s
50 mN/m	150 mlph	0.760s	0.243 m/s
Geometry 2: Nozzle radius 0.4mm			
72.8mN/m	50 mlph	1.8209 s	0.257 m/s
72.8 mN/m	150 mlph	0.667s	0.251 m/s
50 mN/m	50 mlph	1.284s	0.212 m/s
50 mN/m	150 mlph	0.486 s	0.224 m/s

Table 2.2 Results of the simulations, bubble detachment times

Bubble detachment times and rising velocities for each case are given in table 2.2. As it is seen from the table high air injection speed leads to earlier detachment. Injection velocity does not affect the bubble size or dynamics significantly. In all cases after detachment we notice bubble hold up just after the detachment and increase of velocities later. Simulation results are combined as video files and each case were analyzed.

Section 2.4 Validation

In numerical modelling it is important to validate obtained results with experimental data. In literature experiment with bubble growth and detachment for the case with nozzle radius: 0.8 mm and air inlet speed: 150 mlph and surface tension: 72.8 mN/m were analyzed [43]. The growth of bubble at different t/t_{det} times in numerical solution is compared to extracted data from literature. Time over detachment time (t/t_{det}) is a parameter used to identify the growth of the bubble. Sizes of the growing bubble were captured at different t/t_{det} and compared with the experimental data.
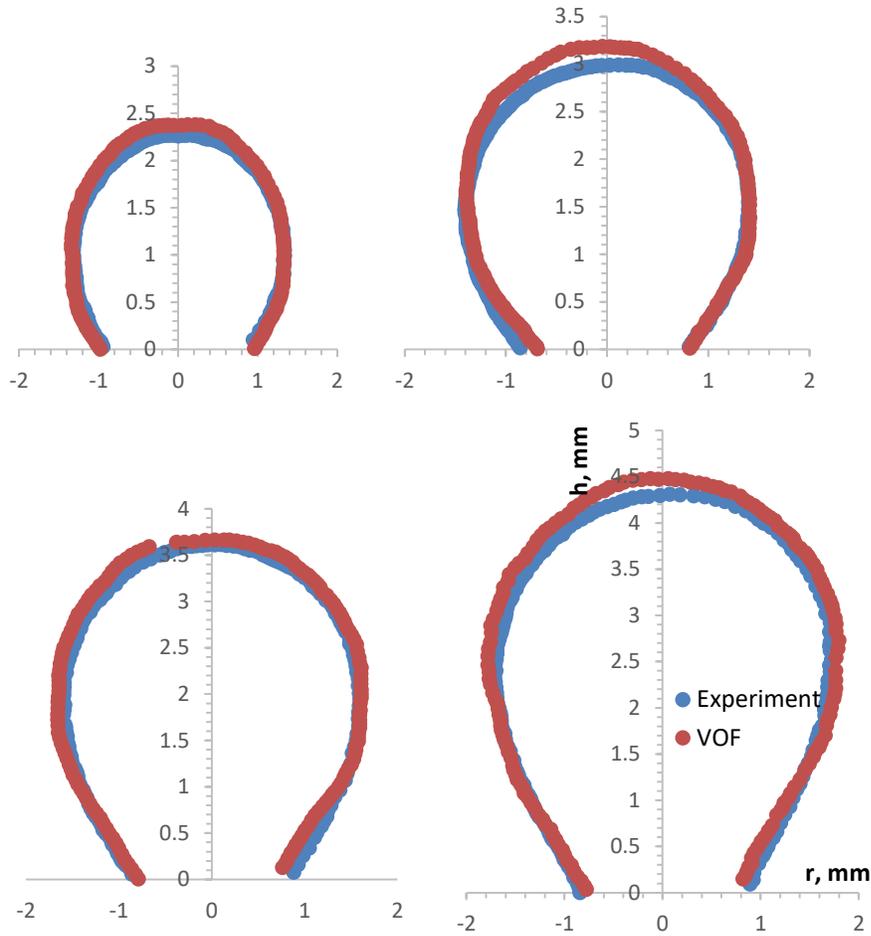
Figure 2.10 Comparison of bubble growth at t/t_{det} = 0.2, 0.4, 0.6 and 0.8, for the case with air inlet speed: 150 mlph, surface tension: 72.8 mN/m, nozzle radius: 0.8mm, VOF simulation against experimental data extracted from literature [43]

Validation of the results of simulation against experimental data's obtained from literature is shown in Figure 2.10. As it is seen from the figure for surface tension 72.8 mN/m and air inlet velocity of 150 mlph bubble growth at the point of t/t_{det}= 0.8, shows compatible results.

Section 2.5 Analysis of the results

Bubble rise velocity theoretically calculated and compared with simulation results. Also Weber and capillary numbers are calculated for each case. The results are shown in table 4. For each case calculation of bubble rise velocities were conducted by extracting bubble coordinates in different time intervals.

For prediction of the bubble velocity Reynolds number is calculated:

$$Re = \frac{\rho u_t D}{\mu} \qquad (2.6)$$

For Re<10^5 the drag coefficient for a bubble is calculated by equation [45]:

$$C_D = [\left(\frac{24}{Re}\right)^2 + 0.44^2]^{1/2} \qquad (2.7)$$

Velocity values obtained from numerical modelling are compared with theoretical. Bubble rising velocity theoretically can be predicted by equation:

$$u_t = \sqrt{\frac{4gD(\rho_p - \rho_g)}{3C_D \rho_g}} \qquad (2.8)$$

As it is seen from table 4 comparison of predicted velocity is close to bubble rise velocity obtained from simulation.

Weber number is calculated by:

$$We = \frac{\rho u^2 l}{\sigma} \qquad (2.9)$$

Capillary number is calculated by equation:

$$Ca = \frac{\mu u}{\gamma} \qquad (2.9)$$

44

In fluid dynamics Weber number is a dimensionless number used to analyze multiphase flows where there is an interface between two different fluids. It is a measure of the relative importance of the inertia compared to its surface tension. Formation of droplets and bubbles are analyzed by Weber number.

Capillary number can be identified as a relative effect of viscous forces versus surface tension at the interface of two different phases, liquid and gas or between two immiscible fluids. Capillary number is a dimensionless quantity and if it is less than 10^{-5} then capillary forces are dominating in the flow. In high capillary number systems capillary forces can be neglected.

Position of the bubble growth and release are determined by tracking the movement in videos generated by simulation results. Center of the mass of the bubble are tracked by use of Matlab software code generated by us for this purposes. Comparisons of the center of mass trajectory by time is given in Figure first and second bubble released from
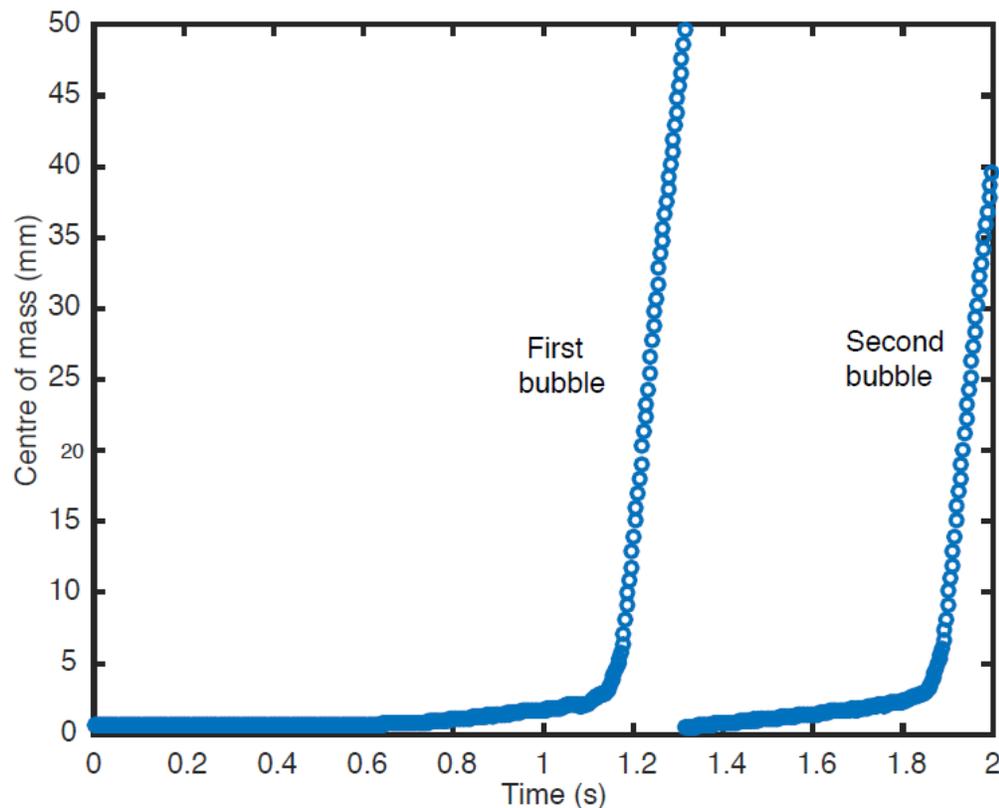
Figure 2.11 Comparison of bubble coordinates of first and second bubble generated in Geometry with nozzle D 0.8 mm, Surface Tension: 72.8 mN/m, Air inlet Velocity: 150 mlph

As it is seen from Figure 2.11 movements of the bubbles look similar. Both bubbles are generated at the same conditions, one after another.

Next it would be interesting to look bubble shapes.
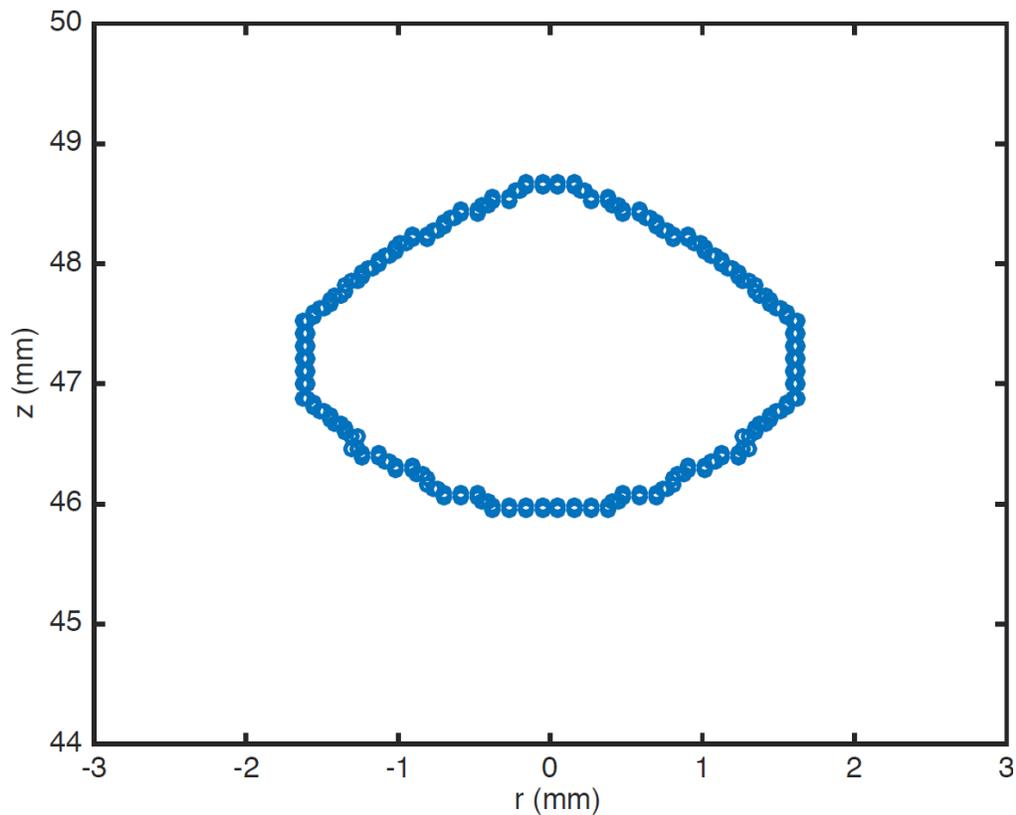
Figure 2.12 Shape of bubble before releasing the tank, obtained from nozzle D:0.8mm, Surface tension: 72.8 mN/m, Air inlet velocity 150 mlph

As it is seen from the comparisons of bubbles, bubble in the system with lower surface tension look more ellipsoidal shaped. Contrary the bubble generated with higher surface tension and larger nozzle diameter look more spherical.
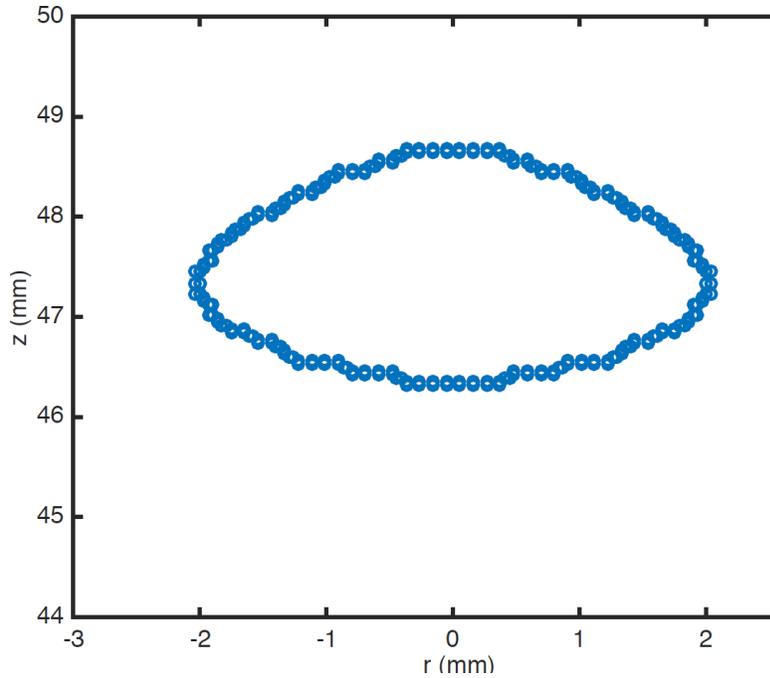
Figure 2.13 Shape of bubble before releasing the tank, obtained from nozzle D: 0.4mm, Surface tension 50 mN/m, air inlet velocity 50 mlph

After analysis of two bubbles generated at different conditions, it is interesting to look to center of mass movement of the bubble by time.
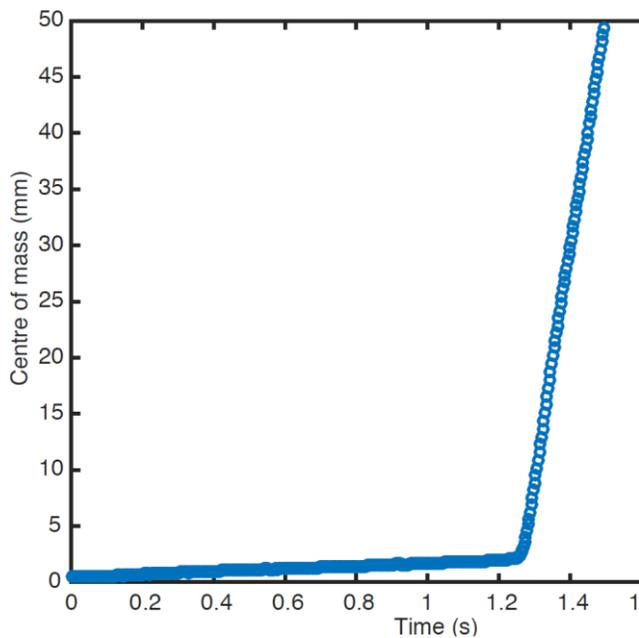
Figure 2.14 Coordinates of center of mass movement of bubble shown above

For every case bubble rise velocity is calculated according to averaged bubble velocity obtained after some point of bubble release. From the velocity values and some other parameters, Reynolds, Weber and Capillary numbers are calculated. Also theoretical value for bubble velocity is calculated and compared to the results from the numerical solution.

Surface tension mN/m	Air inlet velocity mlph	CFD bubble rise velocity m/s	bubble diameter mm	Reynolds number	Weber number	Capillary number	Theoretical predicted velocity m/s (Deviation %)
Geometry 1, nozzle radius: 0.8 mm							
72.8	50	0.252	3.1	781.2	3.94	5.04×10^{-3}	0.303 (16.8%)
72.8	150	0.243	3.3	801.9	1.30	1.62×10^{-3}	0.313 (22%)
50	50	0.222	2.8	621.6	2.76	4.44×10^{-3}	0.288 (22.8%)
50	150	0.234	2.5	585	0.91	1.56×10^{-3}	0.272 (13.9%)
Geometry 2, nozzle radius: 0.4 mm							
72.8	50	0.252	2	504	2.54	5.04×10^{-3}	0.243 (3.7%)
72.8	150	0.251	2.5	627.5	1.05	1.67×10^{-3}	0.272 (7.7%)
50	50	0.221	2.3	508.3	2.25	4.42×10^{-3}	0.261 (15.1%)
50	150	0.219	2	438	0.64	1.46×10^{-3}	0.243 (9.8 %)

Table 2.3: Analysis of theoretical predicted velocity and comparison with simulation results

As it is seen from equations for theoretical velocity calculations input to the equation are bubble diameter and drag coefficient. In this case we assume that the bubbles are spherical. That's why minor deviation from velocities obtained from numerical simulation results might be acceptable.
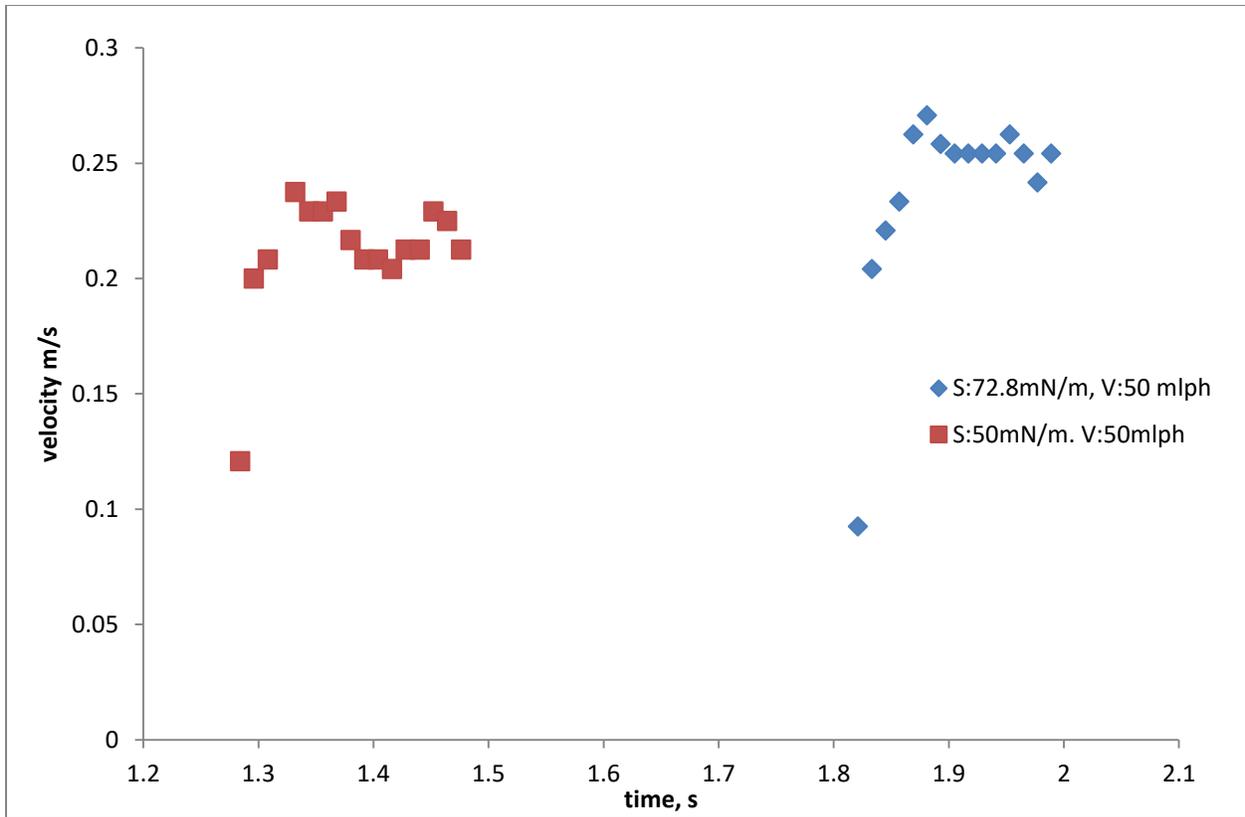
Figure 2.15 Bubble rise velocity versus time after detachment in different surface tensions 72.8 mN/m, 50 mN/m air inlet speed:50mlph, nozzle diameter: 0.4 mm

As it is seen from figure 2.11 bubbles after detachment are generally slow at the beginning and after some time they reach stable velocity. Same trend is monitored for all cases, at the beginning hold up of the bubble occurs and later velocity reaches its maximum. Then when bubbles reach tank boundary we observe decrease of velocities which can be explained by input boundary conditions. Also it can be observed that in the case of 50 mN/m bubble detachment occur sooner than with higher surface tension. Smaller bubbles are generated in the case with less surface tension and bubble rise velocity is slightly lower than compared to the case with higher surface tension.

Chapter 3.Conclusions

Bubble dynamics is indispensable part of the flotation processes. In this thesis we have studied new trends in flotation cell modelling and numerical simulation of air bubble dynamics in liquid phase. Mechanically stirred flotation cell has a complex flow structure and CFD modelling is used to understand the process. Discretization of the whole structure to respective volumes and calculating the fluid characteristics at each volume is a way for its modelling. Also CFD modelling of flotation process is widely used for improving design of the process. Every aspect like location of impellers, input parameters play crucial role in its design and opens door for improvement.

Numerical simulation of bubble growth detachment and rise were modeled for eight different cases to understand effect of air inlet nozzle diameter, air inlet velocity and surface tension of the medium. Obtained results were successfully validated against experimental data obtained from literature and showed good compatibility. For each case bubble rise velocity was calculated and compared to predicted velocity by using theoretical approach. Predicted velocity was in good agreement with simulation results. As it is seen from the simulation results, bubble inlet velocity does not have big effect on bubble size and rise velocity. On the other hand surface tension of the medium and nozzle diameter affects bubble size. In the case with smaller surface tension we get smaller bubbles and less detachment time. Nozzle diameter also affects bubble size, smaller nozzle results with smaller bubble size. It was shown that when nozzle diameter decreased twice bubble size decreases to 20-30 % depending on the case and surface tension of the system. In case with the same nozzle diameter decreasing of surface tension to 30% resulted with the 20% smaller bubble size. From the experiments we can conclude that both nozzle diameter and surface tension are the parameters which can be played to get smaller bubbles. This method is widely used in industry, for flotation process. Different types of surfactants are added to decrease surface tension

of the system, to get smaller and more stable bubbles at froth. Addition of the chemicals to the water for better extraction of the minerals can lead to environmental problems in the long run, that's why, this process should be optimized and added in minimum required amounts. From this view new type of flotation cells are produced with smaller air nozzles for smaller bubble generation.

References

1. A.V.Nguyen (2007) Flotation, *Encyclopedia of separation science*, Elsevier

2. J.Rubio, M.L.Souza, R.W.Smith (2002) Overview of flotation as a wastewater treatment technique, *Minerals Engineering* 15, p.139-155

3. D.A.Deglon, D.Egya-Mensah, J.P.Franzidis (2000), Review of hydrodynamics and gas dispersion in flotation cells on South African platinum concentrators, *Minerals Engineering* 13, p. 235-244

4. V.Lasheva, B. Iliev, S. Kotlarova (2013) Deinking of recycled paper with offset printing through flotation and use of enzymes*, Journal of Chemical Technology and Metallurgy*, 48, 5, p. 530-534

5. R. Miller, L. Liggieri, *Bubble and Drop Interfaces*, CRC Press 2011, p. 352

6. J. Masliyah, J. Czarnecki, Z.Xu (2011) *Handbook on theory and practice of bitumen recovery from Athabasca oil sands, volume 1*, Canada: Kingsley knowledge publishing

7. Z. Xu, Z. Zhou (2013), Flotation Historical Development, Elsevier

8. N. Ahmed, G.J. Jameson (1985) The effect of bubble size on the rate of flotation of fine particles, *International Journal of Mineral Processing*, p.195-215

9. D.R.Nagaraj, S.A Ravishankar (2007) Flotation Reagents- a critical overview from an industry perspective*. Froth Flotation: A Century of Innovation*. USA: SME, Littleton CO, p.375-423

10. L.L.Schramm, R.J.Mikula (2012), *Flotation of Oil Sands Bitumen in Foam Engineering: Fundamentals and Applications*, edited by Paul Stevenson, Wiley

11. R.H.Yoon, G.H.Luttrell (1989), The effect of bubble size on fine particle flotation, *Mineral processing and extractive metallurgy review*, **5,** p.101-122

12. F. Maoming, T. Daniel (2010) Nanobuble Generation and its applications in froth floatation (three parts); *Mining Science Technology* 20, p. 159-177

13. G. Gu, R. S. Sanders , Z. Xu, J. Masliyah (2004) A novel experimental technique to study single bubble-bitumen attachment in flotation, *Int.J.Miner.Process* 74, p. 15-29

14. P.T.L. Koh, M. Manickam, M. P. Schwarz (2000) 'CFD simulation of bubble-particle collisions in mineral flotation cell'. *Minerals Engineering*, 13 , 14-15, p 1455-1463

15. P.T.L. Koh, M. P. Schwarz (2003) CFD moldelling of bubble-particle collision rates and efficiencies in a flotation cell. *Minerals Engineering* 16, p 1055-1059.

16. P.T.L.Koh, L.K.Smith, (2011) The effect of stirring speed and induction time on flotation, *Minerals Engineering* 24, p. 442-448

17. T.Y.Liu, M.P.Schwarz (2009) CFD-based multi-scale modelling of bubble-particle collision efficiency turbulent flotation cell. *Chemical Engineering Science* 64, p 5287-5301

18. M.Kostoglou, T.D.Karapantsious, K.A.Matis (2007) CFD Model for the design of large scale flotation tanks for water and wastewater treatment, *Industrial Engineering of Chemical Research* 46 20, p. 6590-6599

19. C.W.Bakker, C.J.Meyer, D.A. Deglon (2009) Numerical modeling of non-Newtonian slurry in a mechanical flotation cell Minerals Engineering 22, p 944-950

20. T.Y.Liu, M.P.Schwarz, (2008) CFD-based modelling of bubble-particle collision efficiency with mobile bubble surface in a turbulent environment. *Int. J.Miner.Process*.90, p 45-55

21. M. Bondelind, S. Sasic, M. Kostoglou et al. (2010) Single and two phase numerical models of dissolved air flotation, *Colloids and Surfaces A Physicochem. Eng. Aspects* 365, 137-144

22. M. Terashima, R. Goel, K. Komatsu, H. Yasui, H. Takahashi, Y.Li, T. Noike (2009) CFD simulation of mixing in anaerobic digesters *Bioresource Technology* 100 p. 2228–2233

23. S. Shi, M. Zhang, X. Fan (2015) Experimental and computational analysis of the impeller angle in a flotation cell by PIV and CFD *International Journal of Mineral Processing* 142, p. 2-9

24. D.A.Deglon, C.J.Meyer (2006) CFD modelling of stirred tanks: Numerical considerations, *Minerals Engineering* 19 p. 1059–1068

25. M.Karimi, G.Akdogan, S.M.Bradshaw (2014) A computational fluid dynamics model for the flotation rate constant, Part I: Model development, *Minerals Engineering* 69 p. 214-222

26. S. Mitra, E. Dorootchi, V. Pareek, et al. (2015) Collision behavior of a smaller particle into a larger stationary droplet, *Advanced Powder Technology* 26, p. 280-295

27. J.A.Alfaro-Ayala, V.A.Ramirez, A.G.Munoz et al. (2015) Optimal location of axial impellers in a stirred tank applying evolutionary programming and CFD, *Chemical Engineering Research and Design* 100, p. 203-211

28. J. Bridgeman (2012) Computational fluid dynamics modelling of sewage mixing in an anaerobic digester, *Advances in Engineering Software* 44, p.54-62

29. C.W.Bakker, C.J.Meyer, D.A.Deglon (2009) Numerical modelling of non-Newtonian slurry in a mechanical flotation cell, *Minerals Engineering* 22 p.944-950

30. S. Shi, M. Zhang, X. Fan et al. (2015) Experimental and computational analysis of the impeller angle in a flotation cell by PIV and CFD, *International Journal of Mineral Processing* 142, p.2-9

31. G. Hu, I. Celik (2008) Eurlerian-Lagrangian based large-eddy simulation of a partially aerated flat bubble column, *Chemical Engineering Sceince* 63, p.253-271

32. A. Sokolichin, G. Eigenberger (1997) Dynamic numerical simulation of gas-liquid two-phase flows Euler/Euler versus Euler/Lagrange*, Chemical Engineering Science*, 52 4, p 611-626

33. A.Sokolichin, G.Eigenberger (1999) Applicability of the standard k-ε turbulence model to the dynamic simulation of bubble columns: Part I. Detailed numerical simulations, *Chemical Engineering Science* 52, p.2273-2284

34. O. Borchers, C. Bush, A. Sokolichin, G. Eigenberger (1999) Applicability of the standard k-ε turbulence model to the dynamic simulation of bubble columns: Part II: Comparison of detailed experiments and flow simulations, *Chemical Engineering Science* 54, p.5927-5935

35. C.D.Ohl, A.Tijink, A.Prosperetti (2003) The added mass of an expanding bubble, *J.Fluid.Mech*. 282, p. 271-290

36. A.A.Rafiei, M. Robbertze, J.A.Finch (2011) Gas holdup and single bubble velocity profile, *International Journal of Mineral Processing* 98, p.89-93

37. M.van Sint Annaland, N.G.Deen, J.A.M.Kuipers (2005) Numerical simulation of gas bubbles behavior using a three dimensional volume of fluid method, *Chemical Engineering Science* 60, p.2999-3011

38. W. Dijkhuizen, E.I.V. van den Hengel, N.G.Deen, M.van Sint Annaland, J.A.M.Kuipers (2005) Numerical investigation of closures for interface forces acting on single air-bubbles in water using Volume of Fluid and Front Tracking models, *Chemical Engineering Science* 60, p.6169-6175

39. J. Hua, J Lou (2007) Numerical simulation of bubble rising in viscous liquid, *Journal of Computational Physics* 222, p.769-795

40. Abhijit Rao, Rupesh K. Reddy, Franz Ehrenhauser, Krishnaswamy Nandakumar, et al. (2014) Effect of surfactant on the dynamics of a crude oil droplet in water column: experimental and numerical investigation, *The Canadian Journal of Chemical Engineering* 92, p.2098-2114

41. Y.Zhang, A.Samm, J.A.Finch (2003)Temperature effect on single bubble velocity profile in water and surfactant solution, *Colloids and Surfaces* 223, p. 45-54

42. R. Manica, E. Klaseboer, D. Chan (2016), The hydrodynamics of bubble rise and impact with solid surfaces, *Advances in Colloid and Interface Science* 235, p.214-232

43. R.Krishna, J.M. van Baten (1999) Simulating the motion of gas bubbles in a liquid, *Nature* 398, p.208

44. A. Albadawi, D.B. Donoghue, A.J. Robinson et al. (2013) On the analysis of bubble growth and detachment at low Capillary and Bond numbers using Volume of Fluid and Level Set methods, *Chemical Engineering Science* 90 p.77-91

45. L.Bergman, A.S.Lavine, F.P.Incorpera, D.P.Dewitt (2011) *Fundamentals of Heat and Mass Transfer*, 7th Ed., John Willey&Sons.